Review of Permanent-Magnet Brushless DC Motor Basic Drives Based on Analysis and Simulation Study

6 authors, including:

Mehdi Shafiei
Queensland University of Technology
28 PUBLICATIONS   **185** CITATIONS

M. Reza Feyzi
University of Tabriz
96 PUBLICATIONS   **992** CITATIONS

Saeed Danyali
Ilam University
13 PUBLICATIONS   **273** CITATIONS

Mojtaba Bahrami Kouhshahi
Nexteer Automotive
15 PUBLICATIONS   **102** CITATIONS

Some of the authors of this publication are also working on these related projects:

Project   Modeling and Control of Electrical Machine Drives View project

Project   Australian Renewable Energy Agency (ARENA) and industry funded project: Increasing Visibility of Distribution Networks to Maximise PV Penetration Levels View project

Review of Permanent-Magnet Brushless DC Motor Basic Drives Based on Analysis and Simulation Study

S. A. KH. Mozaffari Niapour[1], GH. Shokri Garjan[2], M. Shafiei[3],
M. R. Feyzi[4], S. Danyali[5], M. Bahrami Kouhshahi[6]

Abstract – *Brushless DC (BLDC) motors and their drives have been increasingly considered in a broad range of applications due to their significant features. The implementation of these motors is possible thanks to firstly, the progress of permanent-magnet (PM) technologies which provide high efficiency, power density, and torque for these motors. Secondly, the structure and special features of these motors have prepared a basis for simpler control and smaller size compared to those with the same power. In this paper, the basic drives of BLDC motors have been reviewed in order to provide a useful reference for primary research in conventional methods of these types of motors. To present a proper insight to various drive techniques in these motors a systematic classification to control strategies with principles of these techniques has been made. In addition, computer simulations have been utilized in order to achieve a more accurate evaluation, provide the possibility of comparative analysis between various strategies, and place emphasis on the constraints and features of each method. Apart from the comparison of different methods of each strategy, a general comparison among the different methods of various strategies has been made based on the torque ripple, analysis of frequency, and losses of the BLDC motor drive as well as various applications of the different controlling methods. Moreover, considering the importance of electric vehicles (EVs) in industry, selection of the best controlling method for this type of applications together with energy regeneration has been discussed.* **Copyright © 2014 Praise Worthy Prize S.r.l. - All rights reserved.**

Keywords: *Brushless DC Motor Drive, Current Control, Electric Vehicle, Simulation Study, Torque Control, Voltage Control*

Nomenclature

V_x	Active phase voltage
R	Active phase resistance
i_x	Active phase current
$\psi_{kx}(\theta, i_x)$	Active phase total flux-linkage
$\theta = \theta_e$	Rotor position
$\omega = \omega_e$	Rotor speed
n	Number of motor phases
L	Phase inductance in balanced condition
L_s	Self inductance
L_m	Mutual inductance
V_a, V_b, V_c	Stator phase winding voltages
e_a, e_b, e_c	Stator phase winding back-emfs
i_a, i_b, i_c	Stator phase winding currents
L_a, L_b, L_c	Phase winding inductances
R_a, R_b, R_c	Stator phase winding resistances
p	Number of poles
$k_a(\theta_e), k_b(\theta_e), k_c(\theta_e)$	Phase back-EMF constants
$\psi_{ra}, \psi_{rb}, \psi_{rb}$	Rotor flux-linkages
J	Load and rotor moment of inertia
B	Damping constant
T_L	Load torque
u_d	Dc-link voltage
u_N	Motor neutral point
D	Pulse width modulation duty cycle
$2\Delta I$	Hysteresis band
I^*	Reference current waveform
$I^- = I^* - \Delta I$	Lower hysteresis band
$I^+ = I^* + \Delta I$	Upper hysteresis band
V_{dc}	Inverter dc-link voltage
L_{sw}	Inductor value
f_{sample}	Sampling frequency
$P_{cu-loss}$	Copper losses
H_j	Torque constant
i_a^*, i_b^*, i_c^*	Phase reference currents
I_{Max}	Maximum amplitude of current
$V_{dc-free}$	Applied voltage in build-up region

$V_{dc-built}$	Applied voltage in freewheeling region
T_{free}	Freewheeling time duration
I_0	Initial current value
E'	Back-EMF in commutation interval for on-going phase
E	Peak value of the back-EMF waveform
$k_{\alpha(\theta e)}, k_{\beta(\theta e)}$	Stationary reference frame back-EMF constants
e_α, e_β	Stationary reference frame back-emfs
$i_{s\alpha}, i_{s\beta}$	Stationary reference frame stator currents
$U_{s\alpha}, U_{s\beta}$	Stationary reference frame stator voltages
$\varphi_{s\alpha}, \varphi_{s\beta}$	Stationary reference frame stator flux-linkage
$\varphi_{r\alpha}, \varphi_{r\beta}$	Stationary reference frame rotor flux-linkage
$T_{R-max}, T_{R-min}, T_{ave}$	Maximum, minimum, and average torque value
f_{com}	Commutation frequency
N	Rotor speed in rpm

I. Introduction

In the recent two decades, great increase in energy consumption has brought about environmental problems as a serious concern of the public. In the meantime, the decrease in energy resources, and consequently, the increase on energy costs, has caused many difficulties for numerous countries [1], [2].

Therefore, energy saving technologies have motivated many challenges and have become the most significant and interesting problem. The electric machines performance improvement techniques, as a useful electric tool, can have an effective role in solving the problem [3].

The permanent-magnet (PM) motors technology can be considered as an efficient option due to its high energy generation by PMs which increases the efficiency and also the trade-off which exists between the growth of the manufacturing technology and the decrease in PM costs [4]. The quick growth of variable-speed drives in the automotive industry based on the hybrid drives is a major industry demand in variable-speed PM drives as well [5]. BLDC motors, also known as permanent-magnet DC synchronous motors, are more popular and appealing than other PM motors in energy saving as a result of their better features and performance. Hence, it will be worthwhile to categorize the different controlling strategies of driving these motors and also evaluate the inherent advantages and drawbacks of each method by a comparative analysis and finally, introduce the applications of each.

BLDC motors with a two-phase and/or three-phase supply system, have many advantages over conventional motors; such as better speed versus torque characteristics,

high dynamic response, high efficiency and reliability, long operation life, noiseless performance, high speed range, and low electromagnetic interference (EMI) over induction and DC motors.

The last but not the least, they have higher power to weight and torque to current ratios compared to induction, DC, and PM synchronous motors (PMSMs). It should be mentioned that control of BLDC motor is simpler than induction and PMSM. Thanks to these substantial advantages, BLDC motors are widely utilized in various applications such as industrial automation, aerospace, military, medical, computer, automobile (EV, HEV), and transportation industries, information technology equipment, public facilities equipment, audio-visual equipment, toys, and home appliances in different powers ranging from microwatts to megawatts.

The general structure of a BLDC motor with a six-step inverter is shown in Fig. 1. As seen in Fig. 1, the control structure of this motor is divided into two independent components.
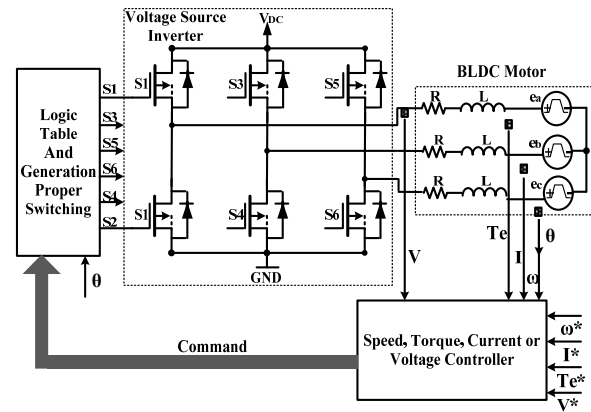

Fig. 1. General structure of the BLDC motor drive with a six-step inverter

The first provides the rotor and stator flux synchronism which is done every 60 electrical degrees by using the rotor position data obtained by a sensor or sensorless techniques and the correct selection of a pair of inverter switches. The second is responsible for producing necessary signals in order to provide desirable control in any of 60 degrees ranges using different controlling strategy such as speed, voltage, current and torque. Speed, current, voltage, or torque can be the aim of controlling strategies in BLDC motors.

The closed loop speed control is used for attenuating speed variations caused by pulsating torques or any other source of disturbance which affects motor desirable speed [6]. In this paper, all the control methods are considered to be equipped with speed control in order to attain a correct comparison and analysis of the mentioned controlling strategies. A speed controller may directly determine the duty cycle of a pulse width modulator (PWM) of a DC-DC convertor as shown in Fig. 2 or be used in a cascade control with an outer speed loop and a current or torque control inner loop. The inner current control may be a PI controller with a PWM or a

hysteresis controller as shown in Figs. 3 and 4, respectively. In addition to current control, hysteresis control is also used for torque control, as shown in Fig. 5.

The first category of the mentioned controlling strategies is voltage control and the second and third categories are current and torque control, respectively. It should be noted that there is another controller called varying input voltage control which is a complementary controller for torque ripple reduction at high speeds.

This control scheme is used with different control methods, in particular, current control as shown in Fig. 6.

This type of controller is placed in the first category due to the direct effect of voltage on motor performance improvement during commutation.
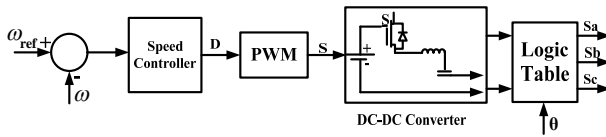

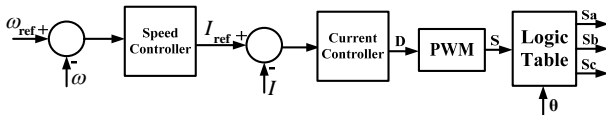Fig. 2. Speed control with variable dc link voltage

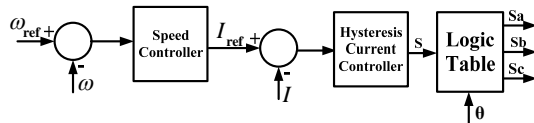Fig. 3. Cascade current control with PWM method

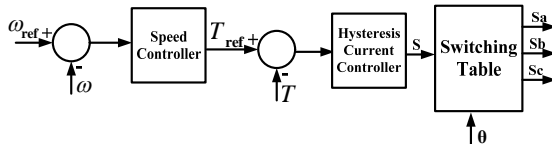Fig. 4. Cascade current control with hysteresis controller

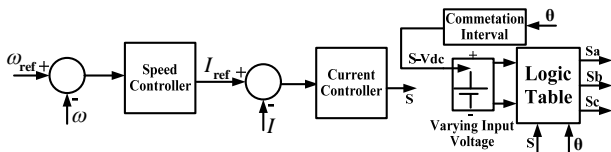Fig. 5. Cascade torque control with hysteresis controller

Fig. 6. Cascade current control with complemented controller (varying input voltage method)

Among the mentioned classification, there is a wide variety for current control category both in reference current generation and PWM algorithms and the type of feedback current extraction. The simplest solution in using feedback current I, is using dc-link current which will not be discussed in this paper due to the following reasons:

- In power inverters, flat cooper plates are generally used between transistors and electrolyte capacitors in order to reduce the inductance between power transistors and dc-link to prevent excess voltages on the switches, which can be dangerous. Thus, it is very hard to connect the current sensor in the dc-link [7].
- Use of a current sensor in a dc-link cannot detect the motor phase currents while they are conducting (during commutation), which results in a greater commutation ripple [8].
- Since the dc-link current is small, it may cause some problems during startup and low speeds, even with high motor currents [9].
- Certain PWM techniques cause floating phase current circulation. These currents result in undesirable utilization of the single current sensor in dc-link [10].
- Dc-link current requires to be sampled according to the switches conduction data; therefore, the system needs complicated calculations with regard to its hardware [11].

II. BLDC Motor

All electric motors that do not require electric connection (made with brushes) between the stationary and rotating components can be considered as brushless PM motors [12]. These motors can be categorized based on the PMs mounted on the rotor and their back-electromotive force (back-EMF) waveform [13].

From a control viewpoint, BLDC motors and BLAC motors have both trapezoidal and sinusoidal back-EMF [14]. In order to maximize the torque density and minimize the torque ripple, it is necessary that either of the motors function in their own operating modes; i.e. BLDC and BLAC phase currents waveform must be rectangular and sinusoidal, respectively [15]. Brushless PM motors can be divided into surface permanent-magnet (SPM) and interior permanent-magnet (IPM) motors based on the PMs mounted on the rotor [16].

BLDC motors are generally considered as brushless PM motors with SPM rotor structure topologies which have trapezoidal back-EMFs and are composed of concentrated non-overlapped stator windings with fractional slots. Since this results in shorter end windings, which is conducive to a high efficiency and torque density in these motors. As previously mentioned, in BLDC motors, the PMs are inset into rotor surface and since magnetic permeability of PMs is near that of air, the air gap in these motors equals the sum of the actual air gap length and the PMs radial thickness, which means small armature field reaction, and consequently, low stator winding inductance [17], [18]. In addition, the d and q axes inductances in these motors are near each other which leads to zero reluctance torque.

This shows that the torque in the BLDC motors similar to that of the separate excitation DC motors, is proportional to the injected current to the motor.

II.1. BLDC Motor Modeling [18]-[21]

Each active phase of BLDC motor can be expressed

by a first order differential equation. The general voltage equation of each active phase is described by:

$$V_x = Ri_x + \sum_{i=1}^{n} \frac{d\psi(\theta, x)}{dt} \quad (1)$$

Flux-linkage in active phase includes both self and mutual flux-linkages. Total flux-linkage of phase A for BLDC motor is given as:

$$\psi_A = L_{aa}(\theta, i_a)i_a + L_{ab}(\theta, i_b)i_b + \\ + L_{ac}(\theta, i_c)i_c + \lambda_{ar}(\theta) \quad (2)$$

where the first term is self-flux-linkage, the second and the third terms are, respectively, mutual-flux-linkage between phases B and C with phase A, and the fourth term is the resultant flux-linkage of the PM on the rotor.

The first three terms in (2) are function of current and position and $\lambda_{ar}(\theta)$ is a function of rotor position. Thus, the flux-linkage level has a close relation with motor dynamic operation.

As previously mentioned, BLDC motors have a very small variation in inductance, so if the motor operates under its rated current conditions, the inductance saturation effect is usually ignored due to the regarded current level. According to SPM specifications of BLDC motors, flux-linkage can be simplified with the following assumptions:

1) Concentrated stator windings are placed with a 120 degree positional difference to each other, and they are connected in wye,
2) Stator winding is symmetric and the winding resistance and inductance are assumed to be constant,
3) Magnetic saturation, hysteresis and eddy current losses are ignored,
4) Armature reaction is ignored and air gap distribution is assumed to be uniform.

According to the above assumptions:

$$\psi_A = L_{aa}i_a + L_{ab}i_b + L_{ac}i_c + \lambda_{ar}(\theta) \quad (3)$$

substituting (3) in (1) gives:

$$V_a = R_a i_a + \frac{d}{dt}(L_{aa}i_a + L_{ab}i_b + L_{ac}i_c) + \frac{d\lambda_{ar}(\theta)}{dt} \quad (4)$$

in balanced BLDC motors:

$$L_{aa} = L_{bb} = L_{cc} = L_s \\ L_{ab} = L_{ba} = L_{ca} = L_{ac} = L_{bc} = L_{cb} = L_m \quad (5)$$

by substituting (5) in (4):

$$V_a = R_a i_a + \frac{d}{dt}(L_s i_a + L_m i_b + L_m i_c) + \frac{d\lambda_{ar}(\theta)}{dt} \quad (6)$$

In this case the following equation is always satisfied by three phase BLDC motor with wye connection:

$$i_a + i_b + i_c = 0 \quad (7)$$

by using (7) and (6); (4) is summarized as:

$$V_a = R_a i_a + (L_s - L_m)\frac{di_a}{dt} + \frac{d\lambda_{ar}(\theta)}{dt} = \\ = R_a i_a + L\frac{di_a}{dt} + \frac{d\lambda_{ar}(\theta)}{dt} \quad (L = L_s - L_m) \quad (8)$$

The last term in the voltage equation is considered back-EMF; thus, the voltage equation is rewritten as below:

$$V_a = R_a i_a + L\frac{di_a}{dt} + \frac{d\lambda_{ar}(\theta)}{dt} = \\ = R_a i_a + L\frac{di_a}{dt} + \frac{d(k_e f_{ar}(\theta))}{dt} = \\ = R_a i_a + L\frac{di_a}{dt} + k_e \frac{d\theta}{dt} \frac{d(f_{ar}(\theta))}{d\theta} \quad (9)$$

It can be recognized from (9) that $\lambda_{ar}(\theta)$ is a constant value which is a function of flux-linkage and varies with rotor position. Thus the three phase BLDC motor voltage equation equals:

$$\begin{bmatrix} V_a \\ V_b \\ V_c \end{bmatrix} = \begin{bmatrix} R_a & 0 & 0 \\ 0 & R_b & 0 \\ 0 & 0 & R_c \end{bmatrix} \begin{bmatrix} i_a \\ i_b \\ i_c \end{bmatrix} + \\ + \begin{bmatrix} L & 0 & 0 \\ 0 & L & 0 \\ 0 & 0 & L \end{bmatrix} \times \frac{d}{dt} \begin{bmatrix} i_a \\ i_b \\ i_c \end{bmatrix} + \begin{bmatrix} e_a \\ e_b \\ e_c \end{bmatrix} \quad (10)$$

since the three phases are similar, therefore:

$$R_a = R_b = R_c = R \quad (11)$$

substituting (11) in (10) gives:

$$\begin{bmatrix} V_a \\ V_b \\ V_c \end{bmatrix} = \begin{bmatrix} R & 0 & 0 \\ 0 & R & 0 \\ 0 & 0 & R \end{bmatrix} \begin{bmatrix} i_a \\ i_b \\ i_c \end{bmatrix} + \\ + \begin{bmatrix} L & 0 & 0 \\ 0 & L & 0 \\ 0 & 0 & L \end{bmatrix} \frac{d}{dt} \begin{bmatrix} i_a \\ i_b \\ i_c \end{bmatrix} + \begin{bmatrix} e_a \\ e_b \\ e_c \end{bmatrix} \quad (12)$$

Electromagnetic torque of a BLDC motor is generated by the stator winding currents and rotor magnet magnetic field interaction which is usually calculated by different

equations as follows:

$$T_{em} = \frac{P}{2}\left[\frac{d\psi_{ra}}{d\theta_e}i_a + \frac{d\psi_{rb}}{d\theta_e}i_b + \frac{d\psi_{rc}}{d\theta_e}i_c\right] =$$

$$= \frac{P}{2}\left[\frac{e_a i_a + e_b i_b + e_c i_c}{\omega_e}\right] = \qquad (13)$$

$$= \frac{P}{2}\left[k_a\left(\theta_e\right)i_a + k_b\left(\theta_e\right)i_b + k_c\left(\theta_e\right)i_c\right]$$

The equation of motion is expressed as:

$$\frac{d}{dt}\omega_r = \frac{1}{J}\left(T_e - T_L - B\omega_r\right) \qquad (14)$$

where J is load and rotor moment of inertia, B is the damping constant, and T_L is load torque.

II.2. Basic Operation Principle of BLDC Motor

BLDC motor uses dc power supply applied by power devices and its switching sequence is determined by rotor position. BLDC motor phase current that basically has rectangular waveform, should be synchronized with the back-EMF in order to produce constant torque in constant speed. In this motor, the conventional mechanical commutator is substituted by power electronic switches and the current of motor windings is supplied as a function of rotor position. This type of ac motor is called brushless dc motor and its operation is similar to conventional dc motors with commutator. Structure of this motor is shown in Fig. 7.
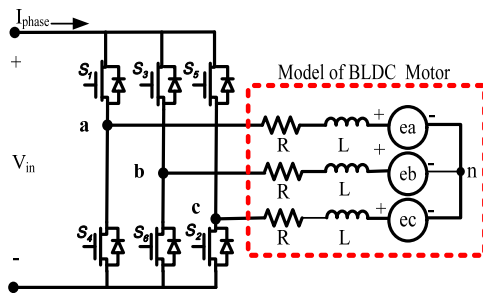

Fig. 7. Configuration of BLDC motor drive system

BLDC motors are generally controlled by means of three-phase inverters so that it requires rotor position sensor for controlling the inverter in order to determine the commutation instants and providing an appropriate sequence for commutation.

The motor position in these motors is generally determined by positional sensors such as Hall-Effect sensors, resolvers, and absolute position sensors; otherwise, it should be prepared by estimation of the parameters specifying the rotor position using sensorless techniques [21], [22]. The conduction range for each phase is usually 120 electrical degrees that is divided to two 60 degree steps; for example, S5-S6, S1-S6, S1-S2, S3-S2, S3-S4 and S5-S4 are six steps of one 360 electrical degree cycle. Therefore, each time only two phases are conducted.

The inverter should conduct every 60 electrical degrees so that the produced currents are in phase with back-EMFs in order to produce the maximum torque [23]. Fig. 8 shows phase current and back-EMF waveforms in 120 degree conduction mode with a six-step pattern for a three-phase BLDC motor.
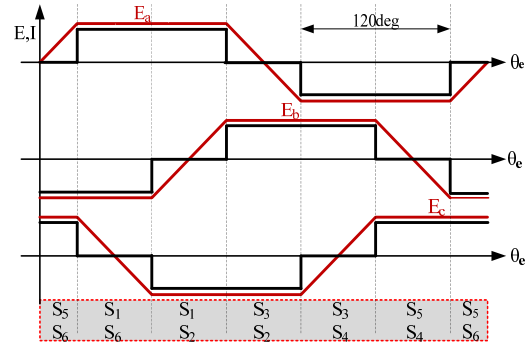

Fig. 8. Phase current and back-EMF waveforms in 120 electrical degree conduction mode with a six-step pattern

III. Current Control Strategies

Current control strategies are the general drive structure for BLDC motors. The main current control strategies can be categorized into three groups based on the controller type, the way of utilization of the sensed currents, and reference currents generation. The controller type group includes two parts: PWM and hysteresis current control approach.

The way of utilization of the sensed currents group also includes two parts: direct exploitation of the sensed currents and exploitation for producing virtual dc-links.

To have a better understanding and comparison between the current control strategies, the aforementioned categorizations are considered more general as PWM and hysteresis current control with and without reference current shaping, minimum copper losses, and current control by exploitation of virtual dc-link. A more detailed description of the mentioned general categories is presented in the following sections.

III.1. PWM Current Control with and without Reference Current Shaping

BLDC motors voltage inverters switching is made by six PWM switching approaches: H-ON-L-PWM, ON-PWM, PWM-ON, PWM-ON-PWM, and H-PWM-L-PWM. PWM operation mode for BLDC motors acts so that the supply voltage is chopped in a constant frequency and a duty cycle dependent on the current error. The mentioned PWM switching approaches are shown in Fig. 9.
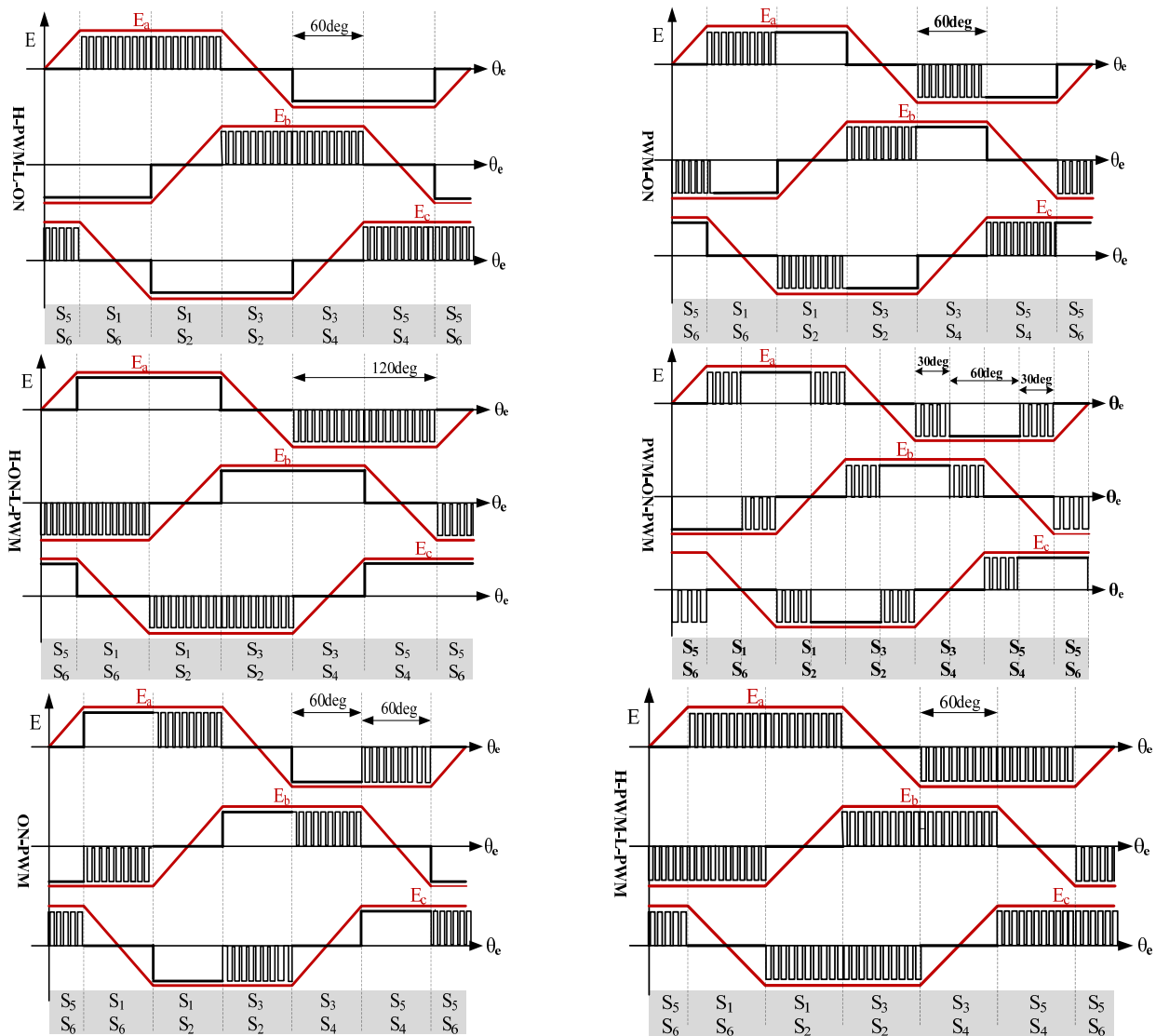
Fig. 9. Logic trigger signals respectively for H-PWM-L-ON, H-ON-L-PWM, ON-PWM, PWM-ON, PWM-ON-PWM, H-PWM-L-PWM modes

All the switching modes are for the 120 electrical degree conduction mode of the motor; i.e. at any instant of time only two phases of the motor conduct and the third phase is off.

In this approach, the switching command is considered as a design parameter and simple filtering of the electromagnetic and acoustic noises and constant switching losses in variable load and speed are the advantages [24], [25]. A drawback of this approach is that triangular wave is hard to produce. In the PWM approaches, H-PWM-L-PWM is called bipolar PWM and considered as hard switching due to the inverter output voltage switch between dc-link voltage and that of the inverse polarity. Other PWM approaches are called unipolar PWM and considered as soft switching since their output voltage switches between dc-link voltage and zero. Since in bipolar PWM approach the two switches under conduction are switched with the desired frequency, the switching losses and current oscillation are

twice that of unipolar approach, but it has faster current dynamic ranging and also its power electronic board design is simpler and cheaper [26], [27].

There exist a linear relationship between current and torque since the back-EMF in BLDC motors is trapezoidal [17], [28]; thus, the current ripple and oscillation in these motors cause ripple and oscillation in torque. The torque ripple is the main cause of vibration and noise in BLDC motors which results in stability degradation and decrease in reliability and also make them useless for the applications in which exact position control is required [29], [30].

Therefore, it is worthwhile to analyze the current dynamic response in different PWM approaches. Hence, the torque ripple in two regions is studied: during the commutation and when conduction occurs. These regions are called commutation region and non-commutation region, respectively.

III.1.1. Torque Ripple Analysis in the Commutation Region

The main task of a motor drive is applying current to the desired windings at the right time and the correct direction. This process in BLDC motors is called commutation which is carried on by inverter switches in order to generate the maximum torque with regard to the rotor position. To analyze the torque ripple in the commutation region it is assumed that phase "a" is going to be turned off, phase "b" is going to be conducted, and phase "c" is being conducted as shown in Fig. 10.

To simplify the equations, we present the following definitions:

$$X = A, B, C \quad (x_1 = a, x_2 = b, x_3 = c)$$

are the stator phase states, $S_x = 1$ and $S_x = 0$ indicate the switching states of the corresponding switch or diode connection on the lower and upper inverter leg, respectively. With the above definitions the equations of inverter phases output average voltage for PWM approaches can be resulted as follows [31]-[33]:

1) H-PWM-L-PWM:

$$u_{x1} = 0 = Ri_{x1} + L\frac{di_{x1}}{dt} + e_{x1} + u_N \quad (15)$$

$$u_{x2} = Du_d = Ri_{x2} + L\frac{di_{x2}}{dt} + e_{x2} + u_N \quad (16)$$

$$u_{x3} = (1-D)u_d = Ri_{x3} + L\frac{di_{x3}}{dt} + e_{x3} + u_N \quad (17)$$

where $i_{x1} = -i_{x2} = i$ and $e_{x1} = -e_{x2} = E$, the neutral point voltage can be obtained by adding (16) and (17):

$$u_N = \frac{1}{2}u_d \quad (18)$$

2) H-PWM-L-ON, PWM-ON and PWM-ON-PWM:

$$u_{x1} = 0 = Ri_{x1} + L\frac{di_{x1}}{dt} + e_{x1} + u_N \quad (19)$$

$$u_{x2} = Du_d = Ri_{x2} + L\frac{di_{x2}}{dt} + e_{x2} + u_N \quad (20)$$

$$u_{x3} = 0 = Ri_{x3} + L\frac{di_{x3}}{dt} + e_{x3} + u_N \quad (21)$$

$$u_N = \frac{1}{2}Du_d \quad (22)$$

3) H-ON-L-PWM, ON-PWM:

$$u_{x1} = 0 = Ri_{x1} + L\frac{di_{x1}}{dt} + e_{x1} + u_N \quad (23)$$

$$u_{x2} = u_d = Ri_{x2} + L\frac{di_{x2}}{dt} + e_{x2} + u_N \quad (24)$$

$$u_{x3} = (1-D)u_d = $$
$$= Ri_{x3} + L\frac{di_{x3}}{dt} + e_{x3} + u_N \quad (25)$$

$$u_N = \left(1 - \frac{1}{2}D\right)u_d \quad (26)$$

According to the (18), (22) and (26) it can be seen that is greater in part (c) approaches than other parts approaches.

By substituting (18) in (15) and (16) and (22) in (19) and (20), and also (26) in (23) and (24), it can be deduced that in the approaches of part III.1.1.1) and III.1.1.3) the falling current slope of phase "a" is greater than the rising current of phase "b".

In the approaches of part III.1.1.2) slopes of falling and rising currents of phases "a" and "b" are the same. This shows that H-PWM-L-ON, PWM-ON, and PWM-ON-PWM approaches substantially have the smallest commutation torque ripple between PWM approaches.
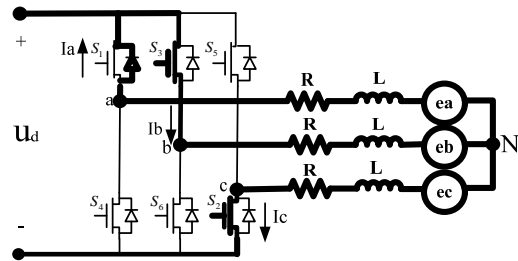

Fig. 10. Current conduction direction while phase "a" and phase "b" are respectively switching off and on and phase "c" is still on

III.1.2 Torque Ripple Analysis in the Non-Commutation Region

The main cause of torque ripple and degradation of control system in the non-commutation region of PWM approaches is the conduction of freewheeling diodes of the inactive phase. Ideally, there must not exist any current in the inactive phase winding. In certain PWM approaches the inactive phase diodes are in on state and connect the inactive phase to the dc-link voltage or zero voltage. The produced oscillating currents into the zero current in inactive phases are called back-EMF current or dc-link reversal current, since they depend on the inactive phase back-EMF value [34]. The dc-link reversal currents cause dc-link voltage to oscillate and decrease the battery life. In addition, they increase with the load

increase and cause more effects [33]. The back-EMF currents have a greater effect on the torque ripple than the commutation currents as they persist longer. In order to analyze and recognize the instantaneous back-EMF currents, it can be written [34]:

$$u_{x1} = u_d s_{x1} = R i_{x1} + L \frac{di_{x1}}{dt} + e_{x1} + u_N \qquad (27)$$

$$u_{x2} = u_d s_{x2} = R i_{x2} + L \frac{di_{x2}}{dt} + e_{x2} + u_N \qquad (28)$$

$$u_{x3} = u_d s_{x3} = R i_{x3} + L \frac{di_{x3}}{dt} + e_{x3} + u_N \qquad (29)$$

by adding (28) and (29):

$$u_N = \frac{1}{2} u_d \left(s_{x1} + s_{x2} \right) \qquad (30)$$

The different resulted states of the motor neutral point instantaneous voltage related to various PWM approaches are as follows:

$$u_N = \begin{cases} 0 & (s_{x1} = s_{x2} = 0) \\ \frac{1}{2} u_d & (s_{x1} = 1, s_{x2} = 0 \ \text{or} \ s_{x1} = 0, s_{x2} = 1) \\ u_d & (s_{x1} = s_{x2} = 1) \end{cases} \qquad (31)$$

Since the analyses are performed in the constant torque region, so the back-EMF value is less than half of the dc-link voltage. The inactive phase voltage is as below:

$$u_{x3} = e_{x3} + u_N \qquad (32)$$

If the inactive phase voltage varies between the dc-link voltage and zero, no back-EMF current will be produced. Thus, to satisfy this condition, (33) is analyzed in both positive and negative back-EMF regions because according to (31) inactive phase voltage depends on the back-EMF value and the neutral point voltage:

$$-e_{x3} < u_N < u_d - e_{x3} \qquad (33)$$

when e_{x3} is positive, to satisfy (33) for the neutral point voltage with regard to switching states, the following equation should be established:

$$\begin{cases} u_N = u_d & (s_{x1} = s_{x2} = 1) \\ u_N = \frac{1}{2} u_d & (s_{x1} = 1, s_{x2} = 0 \ \text{or} \ s_{x1} = 0, s_{x2} = 1) \end{cases} \qquad (34)$$

The above expressed states indicate that among the PWM approaches H-PWM-L-PWM, PWM-ON-PWM, PWM-ON, and H-PWM-L-ON are successful in

eliminating the dc-link reversal currents when e_{x3} is negative similarly the following equation should be established:

$$\begin{cases} u_N = 0 & (s_{x1} = s_{x2} = 0) \\ u_N = \frac{1}{2} u_d & (s_{x1} = 1, s_{x2} = 0 \ \text{or} \ s_{x1} = 0, s_{x2} = 1) \end{cases} \qquad (35)$$

In this case H-PWM-L-PWM, H-ON-L-PWM, ON-PWM, and PWM-ON-PWM are successful in eliminating the back-EMF currents. Results of the performed analyses in this section are shown in Table I with regard to the inactive phase diodes function in different PWM approaches which is dependent on back-EMF value. The block diagram of the PWM current control approach with and without reference current shaping is shown in Fig. 11. The speed feedback derived from the position sensor is compared with the reference speed, and then the reference torque is produced by the PI speed regulator.

In the first case where switch 1 is connected, the instantaneous motor currents are compared with the constant currents produced by the PI controller which are to keep the motor's average speed constant every 120 electrical degrees.

In the second case when switch 2 is connected, proper reference currents are produced in accordance with the predetermined electric back-EMF waveforms in the reference current shaping block and then compared in order to reduce the torque ripple using rotor position.

TABLE I
FREEWHEELING FUNCTION STATES IN PWM MODES
(THE PARENTHESES SIGN REPRESENTS PWM SWITCHING OTHERWISE THE SWITCH IS ON)

Electrical Position of BLDCM to degree		0-30	150-180	180-210	330-360
Back-EMF (+-)		+	+	-	-
H-PWM-L-PWM		(T5)	(T3)	(T3)	(T5)
		(T6)	(T2)	(T2)	(T6)
H-PWM-L-ON		(T5)	(T3)	(T3)	(T5)
		T6	T2	T2	T6
H-ON-L-PWM		T5	T3	T3	T5
		(T6)	(T2)	(T2)	(T6)
ON-PWM		(T5)	T3	T3	(T5)
		(T6)	T2	T2	(T6)
PWM-ON		T5	(T3)	(T3)	T5
		(T6)	T2	T2	(T6)
PWM-ON-PWM		(T5)	(T3)	T3	T5
		T6	T2	(T2)	(T6)
Free Wheeling Diode	H-PWM-L-PWM	D1	×	×	×	×
		D4	×	×	×	×
	H-PWM-L-ON	D1	×	×	×	×
		D4	×	×	✓	✓
	H-ON-L-PWM	D1	✓	✓	×	×
		D4	×	×	×	×
	ON-PWM	D1	×	×	×	×
		D4	×	×	✓	×
	PWM-ON	D1	×	✓	×	×
		D4	×	×	×	
	PWM-ON-PWM	D1	×	×	×	×
		D4	×	×	×	×

In this solution, it is assumed that there is already enough information about motor torque ripple in order to determine the required excitation current waveforms so that the undesired torque can be eliminated.

The reference current shaping method can be performed by either the selected harmonic injection technique or back-EMF inversion [36]-[41].

In this case, the current error can be compared with a triangular wave both directly and after passing the PI controller as shown in Fig. 12. In the first case also known as the ramp comparison method [25], current error can be reduced by adjusting the triangular wave. In the second case, the duty cycle of the corresponding selected PWM approach can be determined by adjusting PI parameters as shown in Fig. 11.
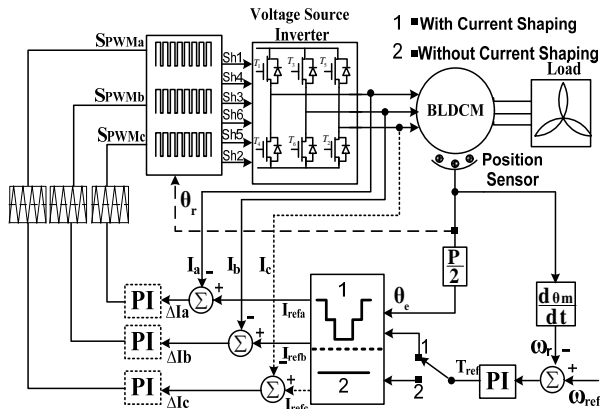

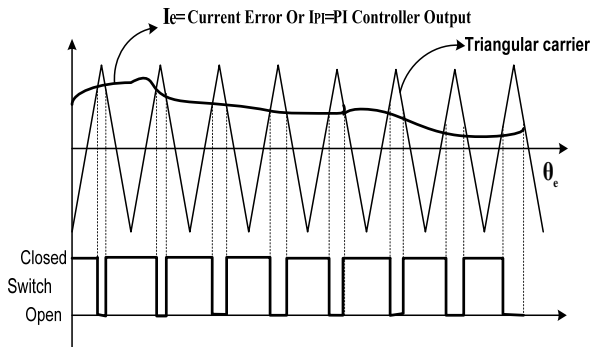Fig. 11. PWM current control approach with or without reference current shaping

Fig. 12. Comparison of error current or PI output with triangular wave and generation of gate signals

To evaluate and verify the discussed issues in this section, especially Table I, different switching algorithms are applied to a standard BLDC motor with the parameters listed in Table II by using the control structure of Fig. 11.

To set the gating signals of the power switches easily and represent the real conditions in simulation as close as possible the electrical model of the BLDC motor with R-L elements and the inverter with power semiconductor switches considering the snubber circuit, the simulation model has been designed in Matlab/Simulink using the SimPower System toolbox. Moreover, the dead-time of

the inverter and non-ideal effects of the BLDC motor are neglected in all the simulation model.

TABLE II
BLDC MOTOR PARAMETER USED FOR SIMULATION

| Parameter	Value	Unit
Number of Poles	2	[pole]
DC Link Voltage	300	[V]
Rated Speed	1500	[rpm]
Phase Resistance	0.4	[Ω]
Phase Inductance	13	[mH]
Load Torque	3	[N.m]
Moment of Inertia	0.004	[kg.m^2]
Torque Constant (V/(rad/s))	0.4	[N.m/A]

The simulations have been performed with a switching frequency of 20 kHz and sampling rate of 50 μs. In addition, all the performed simulations in this section are selected with regard to the control structure shown in Fig. 11 which includes reference current shaping for the ramp comparative method. The waveforms of phase current, electromagnetic torque, and phase-to-ground voltage for six different PWM modes are shown in Figs. 13. In Figs. 13(a) to (d) the dc-link reversal currents and the freewheeling diodes conduction region of inactive phase, which lead to the clamping of the phase voltage, are marked by square and ellipse respectively. In Figs. 13(e) and (f), as predicted, no reversal current is produced since (34) and (35) are satisfied regarding the back-EMF sign; their phase voltages confirm this claim.

Based on Figs. 13 and Table I, It can be inferred that during the upper leg switches' commutation (0-30 degrees) two PWM types, H-PWM-L-ON, ON-PWM, and during the lower leg switches' commutation (180-210 degrees) two PWM types, H-ON-L-PWM and ON-PWM act similarly. Not only do they decrease the maximum value of back-EMF currents' effectively, but the mentioned PWM approaches also act such that the back-EMF currents are suppressed well in advance of the next commutation point.

Hence, these two approaches reduce the destructive effects of back-EMF current on control systems, particularly position sense methods. In the meantime, the PWM-ON-PWM and H-PWM-L-PWM methods completely eliminate back-EMF currents effects, and this result in the increase of the control system's capability and cause the position sense function be without fault in sensorless techniques.

According to the analyses in subsection (III.1.1) and (III.1.2) and Figs. 13, the PWM-ON-PWM approaches have less losses than bipolar PWM and also generate less torque ripple in the commutation and non-commutation range, and have better control capability, the PWM-ON-PWM approach is the best choice between the PWM approaches used in BLDC motors with the same size.

In practice, the specifications of BLDC motors used in unipolar and bipolar PWM drives are different. The back-EMF constant and phase resistance of bipolar PWM drives are twice as much as those of unipolar PWM drives, but the starting torque of both of them is the same.

(a) H-PWM-L-ON

(b) H-ON-L-PWM

(c) PWM-ON

(d) ON-PWM

(e) PWM-ON-PWM

(f) H-PWM-L-PWM
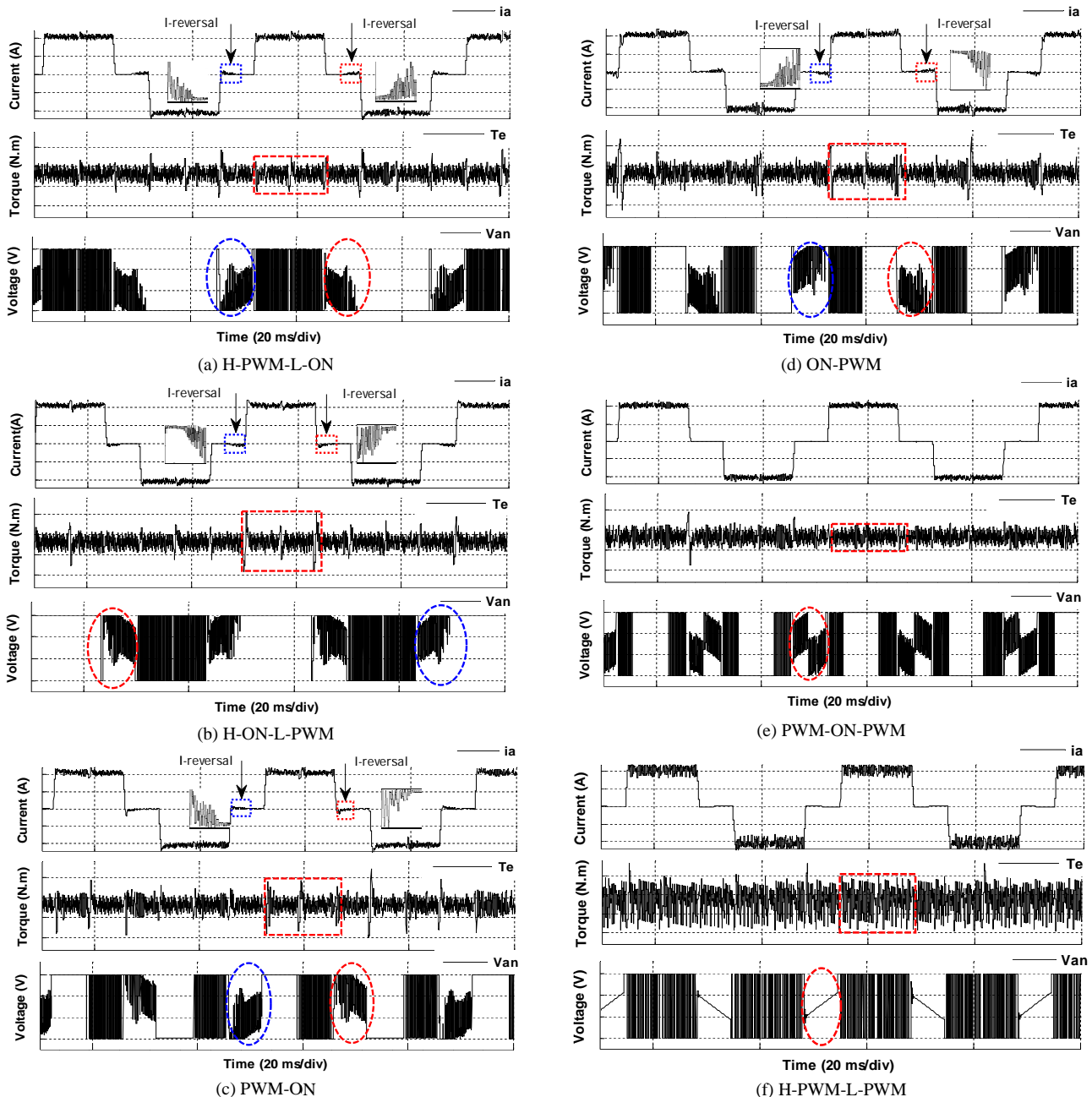
Figs. 13. Waveforms of phase current (upper trace: 2 A/div), electromagnetic torque (middle trace: 0.5 N.m/div),
and phase-to-ground voltage (lower trace: 100 V/div) for six different PWM modes

Unipolar PWM drives are generally utilized at high speeds and in order to reduce the back-EMF voltage drop and prevent the motor from operating in the field-weakening state in high speeds, their back-EMF constant is assigned a smaller value than that of bipolar PWM drives. When a unipolar PWM drive is starting up, it draws great starting current from the motor due to its small back-EMF constant which results in magnetic saturation. This magnetic saturation causes a non-linear speed-current-torque characteristic in BLDC motors and reduces torque constant and back-EMF in these motors [42] and [43].

This means that the startup torque of unipolar PWM drives is practically smaller than bipolar PWM, and if

this drive is used for startup, the motor's efficiency will decrease. Thus, bipolar and unipolar PWM drives are used respectively for startup and high speeds [44] and [45]. Besides, regarding on the performed analyses in this section, for a motor usual operation (not low or high speed), the best PWM approach is selected based on the importance of control behavior.

III.2. Hysteresis Current Control with and without Reference Current Shaping

Hysteresis control is referred to as bang-bang control. Hysteresis current control method is widely used in BLDC motors control due to its simplicity, accuracy, and

acceptable function [46]. Hysteresis current controller ideally has a constant current ripple, but there is no restriction for its switching frequency; however, it is possible to restrict its maximum value using an extra circuit [47].

This control method keeps the motor current in a range around the desired value as shown in Fig. 14 by controlling switching ON and OFF states. When the current tends to exceed the upper band, the corresponding phase connects to the dc voltage source's negative terminal to let the current decrease or discharge.

In a similar manner, when the current tends to exceed the lower band, the switch is closed to let the current pass to increase its amplitude or charge. In BLDC motors, since the back-EMF and the current drawn from the motor are respectively proportional to speed and voltage difference between the dc-link and back-EMF; thus, the current and switching frequency decrease with increase in speed; and at low speeds they increase. However, it is possible to decrease the switching frequency in low speeds by increasing the hysteresis band, but this will increase the torque ripple.

The switching frequency in an inverter controlled by hysteresis varies with the hysteresis band change, the inductor size from which current flows, and the applied voltage to the inductor by the inverter so that maximum switching frequency occurs when the current reference gradient is equal to zero [48]. the maximum value can be obtained by (36) [49], [25], and [8]:

$$f_{sw(max)} = \frac{V_{dc}}{8L_{sw}\Delta I} \qquad (36)$$

This controller can simply be used both digitally and analogically in industry [50].
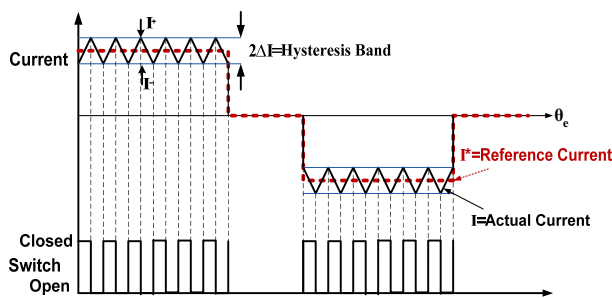

Fig. 14. Hysteresis current controller operation waveform

In an analog system the comparisons are performed continuously, and the current is kept in the assigned band. In digital systems the events occur in discrete intervals. Thus, the sensed currents are digitized and the comparisons are made digitally. In other words, the current information is updated with the sampling frequency of the analog to digital convertor which samples the feedback current.

In this system, it is possible to add the current to the hysteresis band frequently if the sampling frequency is small i.e. the increase or decrease of current continues

until the next sampling time. Therefore, it is of high importance to determine the minimum sampling frequency of the digital system for this type of controllers carefully. The minimum sampling frequency required to obtain an acceptable overshoot is a function of inductance value and its applied voltage. Equation (37) represents the maximum current overshoot for an inverter with a sampling frequency of f_{sample} such that the current ripple is kept sufficiently near the designed value for the analog hysteresis current controller [49]:

$$\Delta I_{over} = \frac{V_{dc}}{8L_{sw}f_{sample}} \qquad (37)$$

The most important aspect of this control method are: adjustable hysteresis bandwidth used to increase control accuracy, difficult electromagnetic noise filtering due to the change of the frequency spectrum component with the switching frequency change, and variable switching frequency at different speeds [51] and [52]. It is more common to use this control method in BLDC motor drives in which speed and load variations are small [21].

Fig. 15 shows the BLDC motor drive strategy with the hysteresis current control method with and without reference current shaping. The reference currents are generated by using processed speed error in PI controller with regard to the explanations given in the PWM approaches section. Then real values of stator currents are measured and compared with the reference currents and the error current is obtained. Finally, by using the rotor position data sensed to improve the commutation and proper switching pattern, all the three hysteresis controllers independently send the required command to the power switches in order to adjust each of the phase currents. It is certainly possible that no position data is sensed for the BLDC motor to operate in three-phase conduction mode. In this case, the error data, alone, is sufficient for the controller.
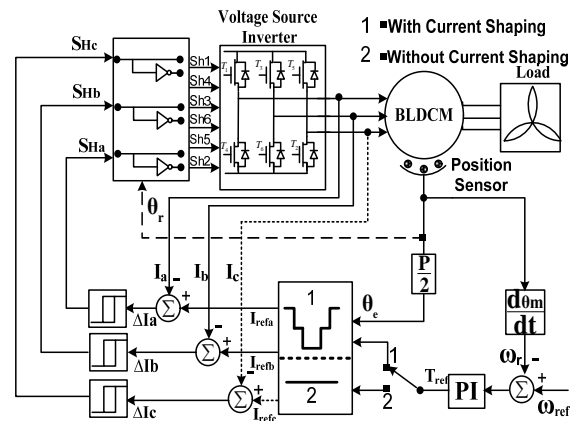

Fig. 15. Hysteresis current control strategy with and without reference current shaping

The simulations in this section have been performed with a sampling time of 50 μs and hysteresis band of 0.24

A, in which the maximum switching frequency and the current overshoot value over the hysteresis band are respectively about 24 kHz and 140 mA calculated through equations (36) and (37). Figs. 16 and 17 show waveforms of the phase current, electromagnetic torque, and phase-to-ground voltage respectively by using with and without reference current shaping strategies obtained from simulation. It is also evident from Fig. 16 that reference current of phase "a" has been generated according to the predetermined back-EMF waveform and the phase current has followed the reference current properly, resulting elimination of torque ripple in low frequency. Although the H-PWM-L-PWM switching algorithms, which are more common, are used in obtaining Figs. 16 and 17, but in the case without reference current shaping, since reference currents are always positive and approximately equal the phase currents' positive value, their switching is practically H-PWM-L-ON, which results in the production of reversal currents and commutation torque ripple; Fig. 17 proves this claim. In addition, Fig. 18 shows waveforms of current, electromagnetic torque, and phase-to-ground voltage with reference current shaping for the three-phase conduction mode. It can be seen from this figure that in this case, the torque ripple is small, but switching losses are large (see Fig. 18(lower trace)).

III.3. Reference Current Shaping by the Minimum Copper Losses Control Method

One of the most important application of BLDC machines is in EV/HEV systems. Traction motors in EV/HEV systems must be selected and controlled so as to provide maximum torque with minimum torque ripple in motor mode and largest power density in generator mode [53].

Since the size and weight of the system has direct effect on fuel consumption and overall efficiency, power density is a significant factor in selecting the type of the required machine.
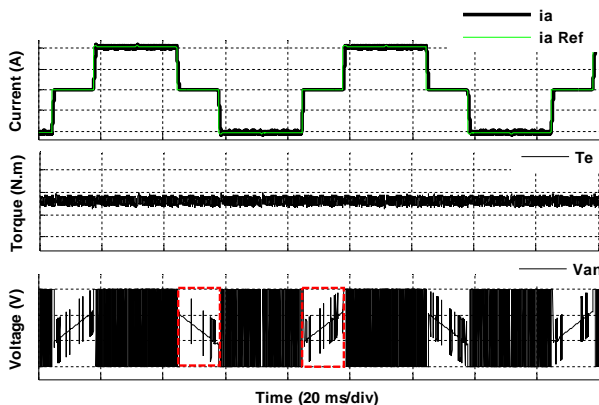

Fig. 16. Waveforms of phase and reference current (upper trace: 2 A/div), electromagnetic torque (middle trace: 0.5 N.m/div), and phase-to-ground voltage (lower trace: 100 V/div) for hysteresis current controller with reference current shaping
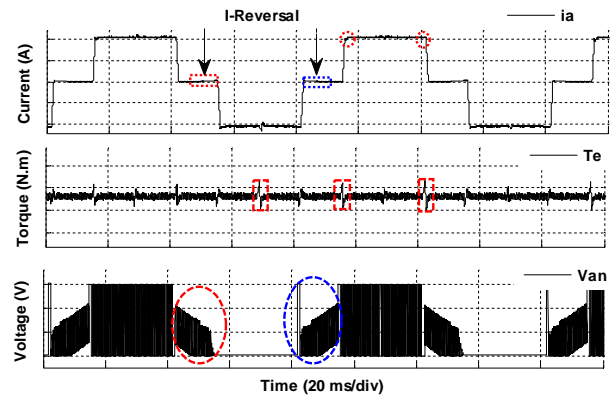

Fig. 17. Waveforms of phase current (upper trace: 2 A/div), electromagnetic torque (middle trace: 0.5 N.m/div), and phase-to-ground voltage (lower trace: 100 V/div) for hysteresis current controller without reference current shaping
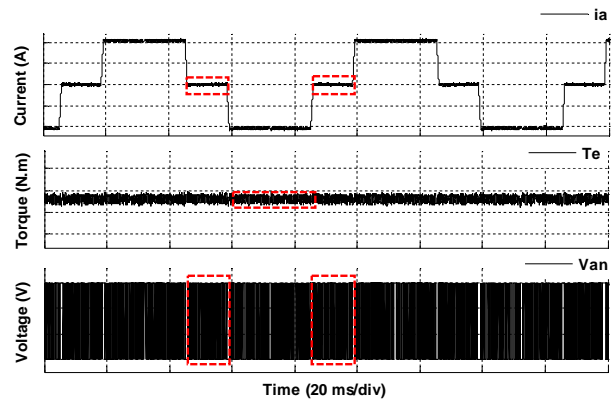

Fig. 18. Waveforms of phase current (upper trace: 2 A/div), electromagnetic torque (middle trace: 0.5 N.m/div), and phase-to-ground voltage (lower trace: 100 V/div) for hysteresis current controller with reference current shaping by using three-phase conduction mode

Employing PMs in BLDC motors, firstly, decreases motor size and weight more than those of other motors with the same power; and furthermore, removing the rotor winding reduces copper losses, increases machine efficiency, improves heat transfer while the motor is more reliable and there is less possibility of damage compared to motors with common windings. This motor can produce higher torque in its current peak value in comparison with other motors [54].

EV/HEV systems generally require propulsion with a high torque and power density, high efficiency, small size, low sound noise, and high driving torque at low speeds and road slope [53]. These features are found in BLDC machines. Thus, major car manufacturers such as Toyota, Honda, and Nissan have started to substitute DC, induction, and switched reluctance (SR) motors with BLDC motors [54]. It is required to reduce the torque ripple in motor mode so as to prevent speed pulsations, vibrations, and motor sound noise as much as possible in order to make this motor a more desirable choice.

Optimal loss control is a simple control method with a fast response for BLDC motors in motor mode which can produce a high average torque and low torque ripple and

copper losses even in three-phase back-EMF unbalanced conditions [53]. This method which is considered a reference current shaping method derives its reference currents from the electromagnetic torque and copper losses equations for a star connection to fulfill the control goals, i.e. copper losses optimization and torque ripple reduction. Equation (13) can be rewritten for electromagnetic torque as follows:

$$T_{em} = H_a i_a + H_b i_b + H_c i_c$$
$$H_j = \frac{e_j}{\omega_r}; \ j = a,b,c \tag{38}$$

instantaneous reference torque is obtained with regard to motor star connection as below:

$$T_{ref} = H_{ba} i_b + H_{ca} i_c \Rightarrow i_c = \frac{T_{ref} - H_{ba} i_b}{H_{ca}} \tag{39}$$

in addition, copper losses is:

$$P_{cu-loss} = R\left(i_a^2 + i_b^2 + i_c^2\right) \tag{40}$$

by substituting (39) in (40) and differentiating from the obtained equation with respect to current and setting it equal to zero, reference currents can be obtained as follows:

$$i_a^* = \frac{2H_{ba} + H_{ca}}{2\left(H_{ca}^2 + H_{ba}^2 - H_{ca}H_{ba}\right)} T_{ref} \tag{41}$$

$$i_c^* = \frac{T_{ref} - H_{ba} i_b^*}{H_{ca}} \tag{42}$$

$$i_a^* = -\left(i_b^* - i_c^*\right) \tag{43}$$

The general structure of the mentioned method is shown in Fig. 19. As shown in Fig. 19, in this method, the reference torque and measured speed of motor are the inputs to the reference current shaping block in order to produce the torque constants and after that, by using the equations presented in this section, reference currents obtained from machine copper losses minimization, are produced as the reference current shaping block output and then compared with the motor's sensed currents.

The obtained error enters the hysteresis current controller and the proper switching command is sent to the switches. The simulations in this section are performed with the same conditions as in the previous section. Simulation results of phase current, electromagnetic torque, and phase-to-ground voltage are obtained by using the current shaping method and copper losses minimization are shown in Fig. 20.

In this control approach, as shown in Fig. 20, there are two noticeable points: first, the peak current value is larger than that of other approaches and current waveform is not square anymore.
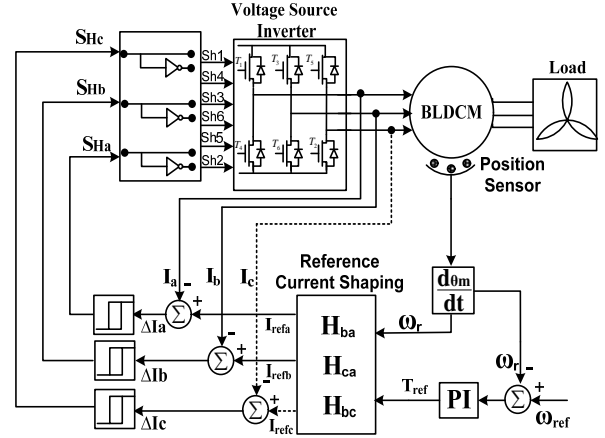

Fig. 19. General structure of BLDC motor for copper losses minimization method
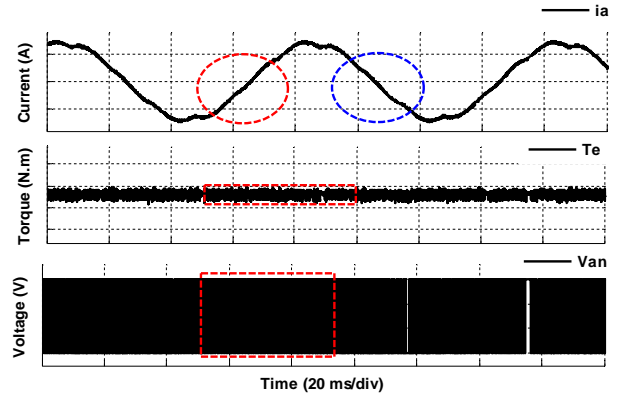

Fig. 20. Waveforms of phase current (upper trace: 2 A/div), electromagnetic torque (middle trace: 0.5 N.m/div), and phase-to-ground voltage (lower trace: 100 V/div) for losses minimization method
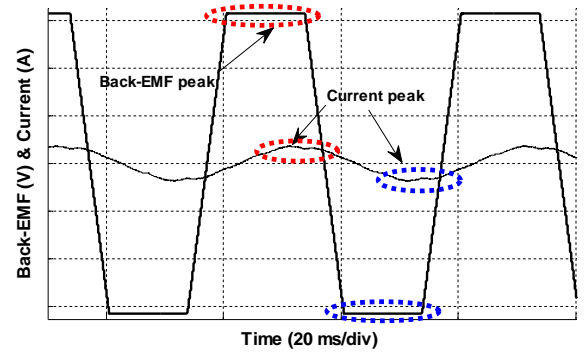

Fig. 21. Phase difference between back-EMF peak and motor phase current peak

Second, switching should be in three-phase conduction mode as verified by voltage waveform (see Fig. 20(lower trace). In addition, since there is a phase difference between the current peak and the flat portion of the back-EMF (Fig. 21), the maximum possible torque cannot be achieved, although the torque ripple is small

due to the incomplete current commutation and operation of the motor with a quasi-sinusoidal current.

The mentioned method is simple and fast and can be applied to motors which have structural defects and unbalanced back-EMF. On the other hand, since a d-q reference or Fourier transformations are not used in this method, complex calculations are not required.

Furthermore, motor efficiency increases, and motor size decreases due to the minimum copper losses achieved in this method.

III.4. Current Control Strategy for Creating Virtual DC-Link

The most common way to control BLDC motors is by means of current controlling of the voltage inverters.

There are three different strategies to exploit the sensed currents in current control drives of BLDC motors. In the first one, phase currents are measured directly by three current sensors and compared with rectangular or constant reference currents in order to trace reference current waveform, as it is verified in the previous sections. Using three current sensors in this strategy for each phase and an extra one for protecting dc-link increases drive expenses.

Furthermore, generating three rectangular waveforms with 120° phase difference is not easily possible, and also motor currents have time delay in relation to generated reference currents, due to time constant caused by winding resistance and inductance, which may lead to disruption of drive operation. On the other side, in this approach it is assumed that sufficient information is already available a priori about the characteristics of the specific BLDC motor to derive the necessary reference current waveforms to achieve the desired torque ripple reduction. The sensitivity of this approach with respect to imperfect knowledge and variations in the motor parameters is other drawback of this scheme.

This strategy is known as reference current shaping strategy or instantaneous current control. Usually this strategy is used in cases in which minimum electromagnetic torque ripple is needed. Having complete information about motor phase currents is substantial in this strategy. A replacement approach for this strategy is using current sensors integrated in power switches in such a way that the currents are adjusted in each phase independently.

However, in this approach, current information is available only when the switches are ON and conducting current. When the switches are OFF, the current passes through the freewheeling diodes, and no information about the current is available [55]-[57]. In the second strategy, only single current sensor is used in dc link to measure phase currents amplitude, I_{Max}. This strategy is the simplest one to drive BLDC motors, but, according to the reasons mentioned in the introduction, this strategy hasn't been presented here. The third strategy, exploiting virtual dc-link [58], is presented to overcome some problems associated with the second strategy.

This approach is based on the fact that the generated torque by BLDC motor is directly proportional to the current. Thus, the inverter should deliver rectangular current with amplitude I_{Max} to the motor according to the load torque [58]. This strategy is depicted schematically in Fig. 22.
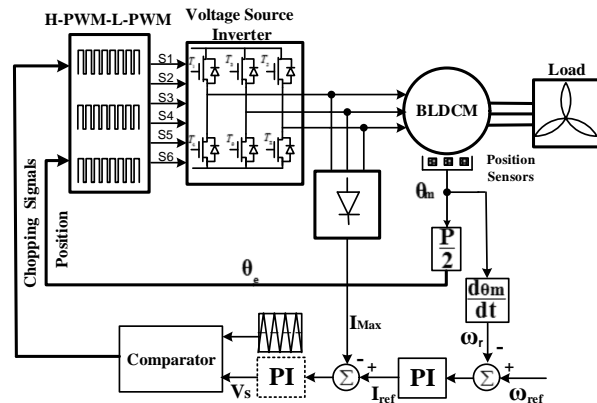

Fig. 22. Schematic depiction of exploiting virtual dc-link strategy

In this strategy, armature's rectangular currents are sensed by means of current sensors and transformed to the voltage signals. These signals are rectified, and the dc components are created with the maximum amplitude of I_{Max} which can be concluded from the relationship in the equation below:

$$I_{Max} = \frac{1}{2} \sum_{k=a,b,c} |i_k| \quad \text{or} \quad I_{Max} = Max \langle |i_k| \rangle \quad (44)$$

I_{Max} is compared with the reference current and produces current error. Then the error signal is passed through the PI controller and is compared with triangular carrier to produce PWM signal and switching is made according to the rotor position.

The simulation has been carried out in this section by switching frequency of 20 kHz, sampling time of 50 μs and H-PWM-L-PWM switching method. Duty cycle adjustment is performed by PI controller. Phase current waveform, electromagnetic torque, and phase-to-ground voltage using current control method in order to exploiting virtual dc-link are depicted in Fig. 23.

The presented control method offers some advantages like simplicity, balanced phased currents, needlessness to measuring dc-link current. On the contrary, in this strategy, rectifiers are used to omit dc-link current sensor, which can increase the drive expenses. On the other hand, torque ripple is still high due to using only single current controller in this strategy as it is demonstrated in Fig. 23.

IV. Voltage Control

IV.1. Variable DC-Link Voltage Controlling

In high speed BLDC motors, suppose a two-pole

BLDC motor with speed of 5000 rpm and PWM switching frequency of 16 kHz. In this motor each 60° which is equal to 200 µs, only 3.2 pulses are used for controlling of speed. Thus, in these motors the commutation delay, the time difference between commutation instant and finishing period of PMW switching, is considerable in relation to motors with a medium speed.
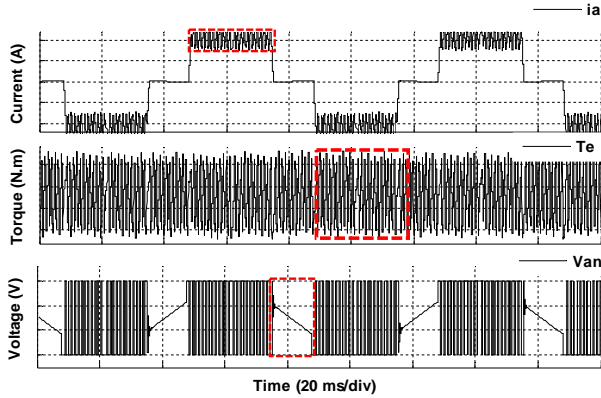

Fig. 23. Phase current waveform (upper trace: 2 A/div), electromagnetic torque (middle trace: 0.5 N.m/div) and phase-to-ground voltage (lower trace: 100 V/div) using current control method in order to exploiting virtual dc-link

Commutation delay causes degradation in the drive performance and has a considerable effect on the phase currents and is responsible for ripple torque which results in changes in the motor speed [59]. To overcome few PWM pulses, in this case, pulse width resolution can be increased considerably, but it can result in speed ripple in steady state and a reduction in the position signal detection accuracy so as it is getting worse along with augmentation in speed.

To solve the second problem, the finishing moment of PWM period and starting instant of commutation signal, should be synchronous. Unfortunately, among all the PWM methods, it is only PWM-ON method which satisfies this condition. In the other PWM methods, commutation delay produces an irregular switching frequency as can be seen in Fig. 24 which leads to a reduction in PWM method attraction.
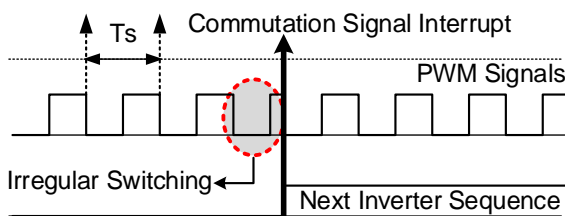

Fig. 24. The relationship between irregular switching and commutation moments

In the BLDC motors with small inductance, by applying PWM to the power switches, current waveform is almost like voltage waveform. Such current waveform

can magnetize and demagnetize motor iron in the PWM frequencies which can lead to magnetic hysteresis losses and thus results in motor extreme thermal losses and damages [60]. Therefore, to overcome the mentioned problems, a special power stage with a variable dc-link is needed [60]-[62]. In this strategy three-phase inverter is responsible for acting correct commutation, while collection of DC-DC converter, inductor L, and capacitor C deal with keeping output voltage at the desired level, illustrated in Fig. 25. In this converter the upper switch only is used to control voltage, and the lower switch is used only in braking state to reduce load voltage level. If the switch is turned on, the inductor is charged and as it is turned off, the energy of inductor is regenerated to the source.

The schematic demonstration of variable dc-link voltage control drive is portrayed in Fig. 25. This controlling method is based on the fact that the commutation ensures motor proper rotation while motor speed is only associated with applied voltage amplitude.

In this controlling strategy, the difference between actual speed and the required one is used as an input for speed PI controller and desired voltage level is acquired.

Then by making a comparison between the voltage level and the measured output voltage of DC-DC converter, the voltage error is applied to the voltage PI controller in such a way that PI controller output determines PWM duty cycle for DC-DC converter excited by inverter and provides voltage amplitude proportional to desired motor speed, whereas commutation algorithm controls commutation frequency according to the rotor position.

The simulation in this part has been performed with sampling time of 50 µs and switching frequency of 20 kHz for DC-DC converter, according to the strategy shown in the Fig. 25.
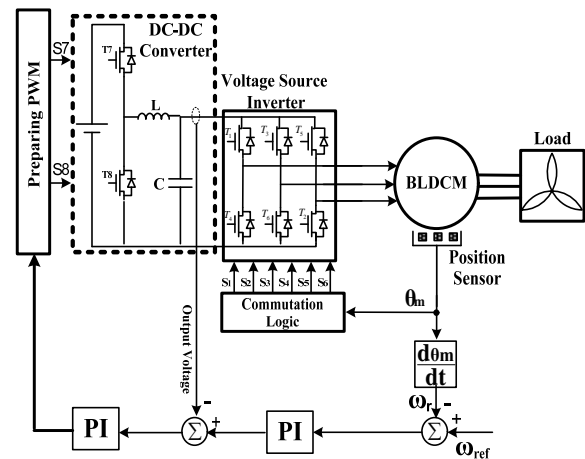

Fig. 25. Schematic demonstration of control drive of variable dc-link voltage

The simulation results for phase current waveforms, electromagnetic torque and phase-to-ground voltage using varying dc-link voltage control strategy are shown in Fig. 26.
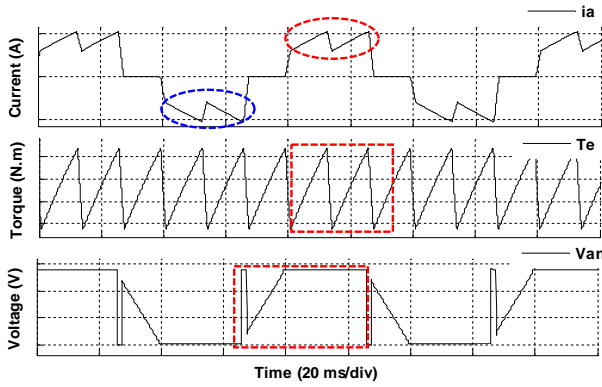
Fig. 26. Phase current waveform (upper trace: 2 A/div), electromagnetic torque (middle trace: 0.5 N.m/div) and phase-to-ground voltage (lower trace: 100 V/div) using variable dc-link voltage control strategy

As it can be seen in Fig. 26, in this controlling strategy, since there are always two power switches ON, inverter cannot produce back-EMF currents as back-EMF value changes. In addition, no current chopping occurs in this strategy in such a way that only harmonics dependent on rotor position are involved. In other words, current and torque fluctuations occur only in the commutation instant in this case.

Thus, terminal voltage includes no frequency harmonic component produced by PWM in this strategy. Subsequently, using this strategy, since no filtering is needed, position detection for sensorless BLDC motors is simpler and more efficient. In addition, the best choice, at high speed, is a linear power stage when switching loss and commutation delay of pulsed power stage is considerable.

However, the major problem involved using this strategy is that sometimes the torque ripple exceeds 50% of its average, as the Fig. 26 verifies.

IV.2. Varying Input Voltage Method

An ideal BLDC motor contains trapezoidal back-EMF, constant input voltage source, and rectangular current.

In ideal conditions, these currents instantaneously reach the steady-state and produce a constant torque for the motor; however, in practice, phase inductance and infinite voltage of the inverter prevents rectangularization of the current waveforms from taking place, in such a way that this issue leads to the distortion of un-commutated phase current in the commutation interval and produces a torque ripple named commutation-torque-ripple. The commutation-torque-ripple is dependent on the current, and its relative width and depth changes according to the speed variations and may reach up to 50% of average torque. From the control viewpoint, the commutation-torque-ripple can be analyzed in two regions, i.e., low-speed region ($V_{dc} > 4E$) and high-speed region ($V_{dc} < 4E$) [64].

The aim of applying any controller in the commutation interval is to keep the un-commutated

phase current constant for reducing the commutation-torque-ripple. As the motor is operating at low-speed, the rising current increasing rate can be reduced during the commutation interval by chopping the corresponding phase current so that the rising and falling currents variation rate amount to each other and reach their steady-state values at the same time, and consequently prevent from producing torque spikes.

Likewise, as the motor is operating at high-speed, the falling current decreasing rate which coincides with the conducting freewheeling diodes during the commutation interval could make a delay in the falling phase current by utilizing a three-phase conduction mode in the commutation interval in order that the production of torque dips could be prevented. In fact, in such a state, the uncontrolled falling phase current changes into a controllable current for the motor via the freewheeling diodes by utilizing the chopping of all the three phases.

Other conventional methods [65] and [66] have both used duty cycle pulse width modulation (PWM) variation during the commutation interval which is somehow based on average voltage variation applied to the motor in the commutation interval to overcome the commutation-torque-ripple.

Unfortunately, the duty cycle PWM variation methods or, all in all, the methods which are not based on varying dc-link voltage, act unsuccessfully in increasing the rising phase current rate for some of the operating conditions of the motor, for example, at high-speed operation even by the full exploitation of the dc-link voltage. Nevertheless, while the motor is operating at low-speed, the conventional methods of the BLDC motor drive can more or less keep the un-commutated phase current constant, so it is really important that the high-speed operation of the BLDC motor, which leads to that the unwanted subsequent switch, which takes command from the position of appropriate rotor speed, act before reaches its steady value, be controlled.

One of the efficient ways of reducing commutation ripple torque, which has been recently presented, is varying input voltage controlling method [67]. This method uses circuit analysis in Laplace domain during commutation interval. Commutation region in this method, as can be seen in Fig. 27, is divided into two regions; freewheeling and build-up.
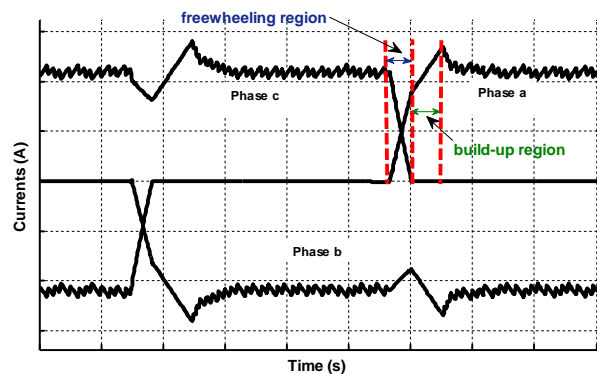

Fig. 27. Freewheeling and build-up region in a commutation interval

While the commutation is occurring from phase *c* to phase *a*, current ripple cannot be generated in case current of phase *a* is constant.

In other words, the commutation-torque-ripple can be reduced by keeping the un-commutated phase current constant in the freewheeling region and applying of varying direct current voltage instead of dc voltage with fixed amplitude. Supposing the commutation is occurring from phase *c* to phase *a*, Figs. 28 show the system equivalent circuit in the Laplace domain for the two regions, freewheeling and build-up. As it can be understood from Fig. 27, all the three phases are conducting the current during the commutation interval as long as the phase current, whose switch has been off, does not decay to zero.

In this interval, a getting-off phase of the motor lies parallel to the getting-on phase, that is why the off-phase freewheeling diode current drops faster than on-phase current, the issue which causes the generation of the commutation-torque-ripple. As the off-phase current is decaying to zero, the build-up region starts in the two on-phases by the, in this case, if the electrical period of the BLDC motor rotation is shorter than the time constant of the on-phase current, the current cannot reach its steady-state value bounded by resistance, and this region will also be a factor for generation of the current ripple and torque.

In this method, instantaneous voltages and currents can be calculated using circuit analysis in the Laplace domain (see Figs. 28) as well as applying Kirchhoff's laws in each of the equivalent circuits.

Finally, the current ripple and commutation torque can be reduced varying input voltage during the freewheeling interval which has been expressed in equations (45)-(47), respectively.

$$V_{dc-free} = 3RI_0 + 3E + E' \quad (45)$$

$$V_{dc-build} = 2(RI_0 + E) \quad (46)$$

$$T_{free} = -\frac{L}{R}ln\left(\frac{3V_{dc-free} + 2E'}{9RI_0 + 3V_{dc-free} + 2E'}\right) \quad (47)$$

The conducted simulations in this part have been performed by sampling time of 50 μs and hysteresis band of 0.16 A for performance rate of 2500 rpm.

The simulation results for waveforms of phase currents and electromagnetic torque using hysteresis current controlling with reference current shaping without and with varying input voltage controlling method, respectively, are illustrated in Figs. 29(a) and (b). As it can be seen from Fig. 29(a), the controller cannot resist commutation current ripple of the motor at high speed during commutation even by applying the desired current controlling method for reducing torque ripple, and it has been caused a big and unwanted commutation torque ripple for the motor. This is where, by applying complement method of varying input voltage

and current controlling method which has been mentioned before, as it can be seen in the Fig. 29(b), by applying variable input voltage in the commutation interval which can be seen in the figure by dashed line, current ripple in the commutation interval and therefore motor commutation torque ripple has been decreased greatly.
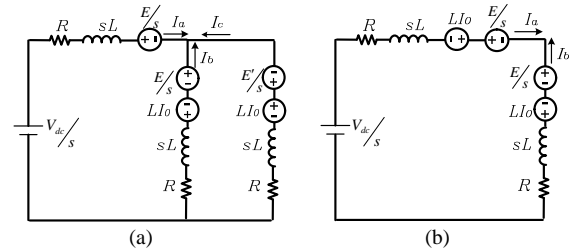
Figs. 28. Equivalent circuit using Laplace transform in: (a) freewheeling region (b) build-up region

(a)

(b)
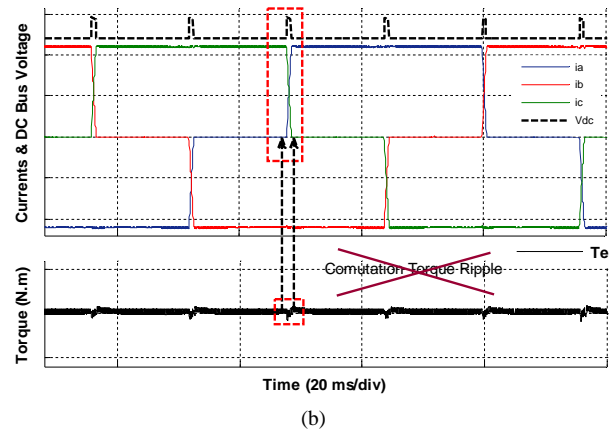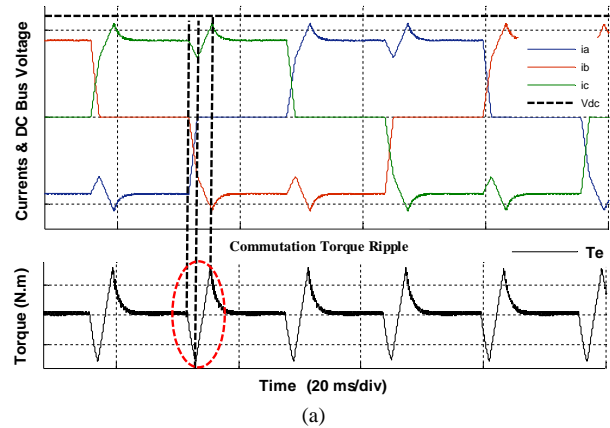
Figs. 29. Voltage waveform of dc bus (upper dashed line trace: 125 V/div), phase currents (middle trace: 2 A/div), electromagnetic torque (lower trace: 0.5 N.m/div): a) without using varying input voltage method b) using varying input voltage method

Varying input voltage controlling method is a complement method which is very efficient in reducing commutation torque ripple at high speed. This method is feasible usually by change of dc bus voltage which practically is carried on by means of DC choppers or by fire angles controlling of rectifier switches. One of the

major problems associated with this controlling method is that commutation occurring period must be given accurately to make the controller act correctly, and it can increase drive expenses greatly.

V. Direct Torque Control of BLDC Motor Using Two-Phase Conducting Mode

In the direct torque control method (DTC), a combination of vector control and direct self-control theories is used to achieve an appropriate drive with practical variable frequency [68], [69].

In this control method, direct control of stator flux and electromagnetic torque, and attainment rapid torque response and the high efficiency is possible by choosing the efficient modes of switching inverter to confine flux and torque error in a proper hysteresis band. Correct torque estimation is the key point in the DTC method in the constant torque region to drive a BLDC motor.

For a BLDC motor with non-sinusoidal (trapezoidal) back-EMF, without considering two-phase or three-phase conducting mode, electromagnetic torque can be calculated using stationary reference frame as (48) [70]-[73]:

$$T_{em} = \frac{3}{2}\frac{p}{2}\left[\frac{d\psi_{r\alpha}}{d\theta_e}i_{s\alpha} + \frac{d\psi_{r\beta}}{d\theta_e}i_{s\beta}\right] =$$
$$= \frac{3}{2}\frac{p}{2}\frac{1}{\omega_e}\left[e_\alpha i_{s\alpha} + e_\beta i_{s\beta}\right] = \qquad (48)$$
$$= \frac{3}{2}\frac{p}{2}\left[k_{\alpha(\theta_e)}i_{s\alpha} + k_{\beta(\theta_e)}i_{s\beta}\right]$$

Since the last term in (48) does not contain rotor speed in the denominator, there will be no problem for torque estimation in zero and near zero speeds. Therefore, using this torque term in the control method is helpful.

Stator flux-linkage vector can be determined by measuring stator voltages of $\alpha\beta$ axis, $U_{s\alpha}, U_{s\beta}$, and $i_{s\alpha}, i_{s\beta}$ currents as follows:

$$\varphi_{s\alpha} = \int\left(U_{s\alpha} - R_s i_{s\alpha}\right)dt \; , \; \varphi_{s\beta} = \int\left(U_{s\beta} - R_s i_{s\beta}\right)dt \quad (49)$$

The magnitude and angular position of stator flux-linkage vector can be calculated as follows:

$$\varphi = \sqrt{\varphi_{s\alpha}^2 + \varphi_{s\beta}^2} \quad , \quad \theta = tan^{-1}\frac{\varphi_{s\alpha}}{\varphi_{s\beta}} \qquad (50)$$

The rotor flux-linkages can be deduced from the stator flux-linkages and are given by:

$$\varphi_{r\alpha} = \varphi_{s\alpha} - L_s i_{s\alpha} \; , \; \varphi_{r\beta} = \varphi_{s\beta} - L_s i_{s\beta} \qquad (51)$$

Basic operation blocks used to implement DTC scheme core are illustrated in Fig. 30. Four impressive

blocks to provide required prime control are: speed controller, flux and motor torque estimator, torque, and flux comparators, and switching logic which determines inverter switching status.

Flux and torque estimators are responsible for feedback signal production or estimation such as real stator flux, generated torque and stator flux position. Torque and flux comparators contain hysteresis control blocks which are designated to compare command torque and flux with their actual values. Speed feedback derived from rotor position sensors is compared with reference speed and command torque is gained using speed PI controller. Electromagnetic torque and stator flux linkage commands are derived by comparing their actual with their corresponding demanded values are given by hysteresis controller.

As it can be understood from Table III, inverter switching pattern is according to the torque status and stator flux-linkage which can be determined by the outputs of the two regulators shown in the Fig. 30 and also determined sectors by stator flux at any instance of time. Since only two phases are excited and controlled in BLDC motor driving within each $60°$, if real stator flux-linkage value is equal to the reference stator flux-linkage in each sector, a non-zero voltage space vector, as can be seen in the Table III, is used to increase or decrease torque value.

In addition, when actual flux-linkage is lower than its reference value, a non-zero voltage space vector is used to increase flux-linkage, when actual flux-linkage is bigger than its reference value, another non-zero spatial voltage vector is used to decrease stator flux-linkage.

Processing flux and torque output status, which is a function of optimal switching logic to choose appropriate stator voltage vector, is performed by voltage selector to satisfy flux and torque output. Actually, in this method there are only six non-zero stator voltage vectors that voltage inverter can produce for BLDC motor drive.

Nevertheless, in the direct torque controlling method, flux controller can be omitted from BLDC motor drive in the constant torque region due to the following reasons [73]-[76]. First, since in the constant torque region, back-EMF amplitude is smaller than half of dc-link voltage, stator flux-linkage amplitude is approximately constant, so no flux amplitude controlling is needed. Second, in the two-phase conducting mode, in the commutation intervals, sudden sharp dips occur in the stator flux-linkage locus. The size of these sharp dips is completely unpredictable and depends on different parameters like sampling time, dc-link voltage, hysteresis bandwidth, snubber circuit, motor parameters specially winding inductance, motor speed and torque value, so it is very difficult to control it. Third, since stator flux waveforms are not sinusoidal, d-q transformation and consequently flux amplitude controlling cannot be performed correctly. Fourth, regardless of the stator flux-linkage amplitude, the phase currents instinctively inclined to adapt themselves with the flat top portion of the corresponding trapezoidal back-EMF to generate constant torque.

So, using DTC method to drive BLDC motor, flux error F_{st} in choosing voltage vector in look-up table is always considered as zero and only torque error T_{st} which depends on actual torque error level in relation to command torque is used. As it can be seen in Table III, if command torque is bigger than actual torque in the hysteresis band, torque error T_{st} is indicated with T_I; otherwise, it is indicated with T_D. The overall block diagram of the DTC scheme of a BLDC motor drive is represented in the Fig. 30.

The gray region in the figure represents stator flux-linkage control part which is brought only for comparison purposes. If the indicated key in the Fig. 30 toggles from status 2 to status 1, flux control in the whole system is considered with torque control. Fast torque response, small torque ripple, simple algorithm, and simplicity in applying it to the motor are the most important advantages associated with this controlling method.

Conducted simulations in this part have been performed with sampling time of 5 μs and hysteresis band of 0.1 N m, and no flux controller has been considered. Simulation results for phase current waveform, electromagnetic torque, and phase-to-ground voltage using DTC strategy are shown in the Fig. 31. Since electromagnetic torque is proportional to multiplication of back-EMF and its equivalent current, phase currents are formed automatically and efficiently

in order to earn desired electromagnetic characteristic corresponding to (48).

As it can be inferred from Fig. 31, it has been caused low-frequency torque ripple to be omitted. High-frequency ripple observed in the torque and current figures are related to controllable factors like sampling time, hysteresis bandwidth, winding inductance and, dc-link voltage.

As it can be deduced from current and voltage waveform, no reversal current exist; the reason is efficient switching of DTC method, which prevents producing any reversal current. It should be mentioned that smoother electromagnetic torque can be earned by pre-storing actual stationary reference frame of the back-EMF constant waveforms.

VI. Discussion

Torque ripple: Torque ripple controlling in the BLDC motors is the most important purpose of high performance systems that should be investigated to minimize perturbations like acoustic noise, vibration, speed fluctuation, and degradation in the drive performance.

Therefore, first torque generation factors should be recognized, and their main sources should be introduced. Torque generation factor can be divided into two general categories; cogging torque and torque ripple.
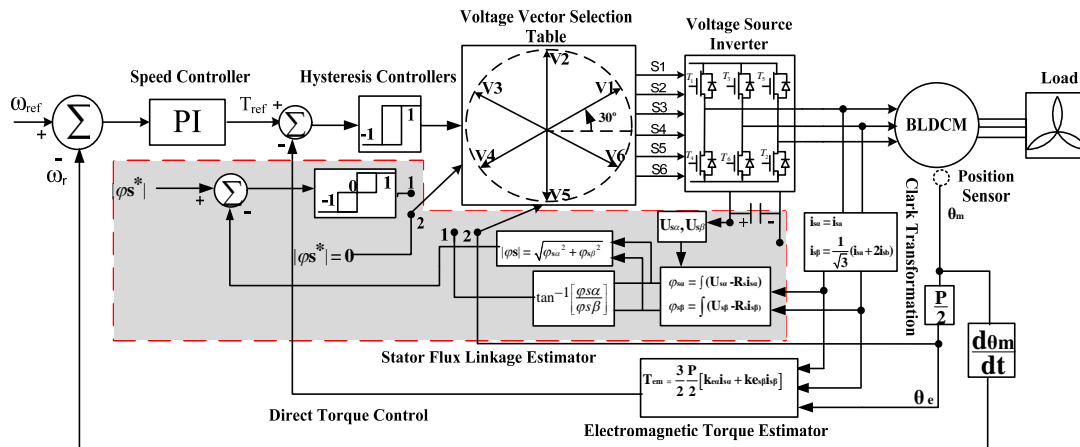

Fig. 30. Overall block diagram of the DTC of a BLDC motor drive in the constant torque region

TABLE III
CHOOSING SWITCHING STATUS FOR USUAL THREE-STATE DTC ARE: TI TORQUE INCREASING, TD TORQUE DECREASING,
FI FLUX INCREASING, FD FLUX DECREASING AND NO CHANGING IN F FLUX

Fst	Tst	Sector					
		Θ1	Θ2	Θ3	Θ4	Θ5	Θ6
FI	TI	V1(100001)	V2(001001)	V3(011000)	V4(010010)	V5(000110)	V6(100100)
	TD	V6(100100)	V1(100001)	V2(001001)	V3(011000)	V4(010010)	V5(000110)
F	TI	**V2(001001)**	**V3(011000)**	**V4(010010)**	**V5(000110)**	**V6(100100)**	**V1(100001)**
	TD	**V5(000110)**	**V6(100100)**	**V1(100001)**	**V2(001001)**	**V3(011000)**	**V4(010010)**
FD	TI	V3(011000)	V4(010010)	V5(000110)	V6(100100)	V1(100001)	V2(001001)
	TD	V4(010010)	V5(000110)	V6(100100)	V1(100001)	V2(001001)	V3(011000)

Italic grey region has not been used in applying DTC method to drive BLDC motor.
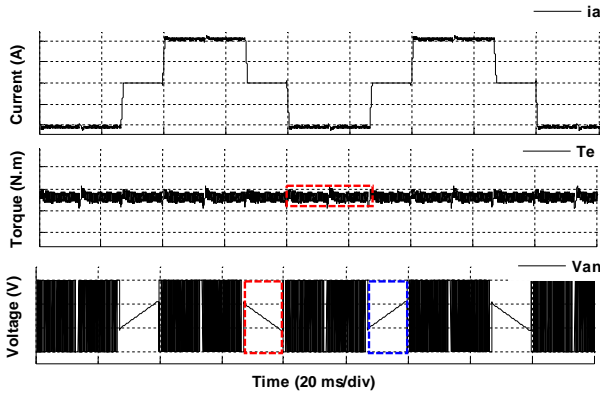
Fig. 31. Phase current waveforms (upper trace: 2 A/div), electromagnetic torque (middle trace: 0.5 N.m/div) and phase-to-ground voltage (lower trace: 100 V/div) for direct torque controlling method

Cogging torque is produced by mutual interactions of PM and stator slots and teeth while torque ripple can be created by reluctance and mutual torque that the first one is produced by angular changes in rotor magnet reluctance, and the second one is produced by mutual coupling between stator winding current and rotor magnetic field [30] and [6]. Since BLDC motor rotors are SPM, reluctance torque component is minimum and can be ignored.

From the designing point of view, generated fluctuations in the first stage can be reduced by improving the motor designing characteristics or motor geometry correction using methods like skewing stator teeth or rotor magnet poles, notching in teeth, shifting magnet poles, and optimization of pole arc to pole pitch ratio [76]-[79]. It should be mentioned that generated parasitic fluctuations in this stage cause back-EMF distortion in its ideal waveform. From the drive point of view, mutual torque fluctuation in the BLDC motors can be categorized in two groups: torque-free-ripple and commutation-torque-ripple.

Totally, each source that results in a separation between drive, power converter and their ideal characteristics can produce unwanted torque fluctuations. Important cases in this field can be pointed out to excitation current waveform distortion due to inverter commutation, controller, and motor performance at high or low speed, low resolution or offset in measuring a quantity, delay in synchronism between excitation current, and rotor position.

One of the most efficient and most dominant procedures to minimize generated torque fluctuations by cogging torque is done through proper design of BLDC motor. There are many instances for them, not only motor designing methods are not sufficient, but also using proper motive control drive is needed to minimize torque ripple. Therefore, cogging torque fluctuations effects are not considered in this paper, that is, in all the verified drive methods in the previous parts back-EMF has been considered ideal and trapezoidal, and reasons and causes of generated torque fluctuations associated with drive have been investigated under this condition.

Thus, in order to make a comparison and gain a comprehensive understanding of controlling strategies discussed earlier from the torque ripple point of view, a table corresponding to Table IV has been prepared in which average torque and sampling time are considered 3.3 N.m and 10 μs, respectively. The ripple torque in this table is defined in brief as below:

$$T.R. = \frac{T_{R-max} - T_{R-min}}{T_{ave}} \times 100 \qquad (52)$$

Maximum and minimum torque values are considered in a period in Table IV. The result presented in the table shows that hysteresis current control methods with reference current shaping with two-phase or three-phase conducting mode, DTC and hysteresis current control with reference current shaping using copper loss minimization method are the best methods to reduce torque ripple of the motor in normal condition. These methods using their high controlling ability are able to improve ripple torque around 40% in comparison with variable dc-link voltage method. Besides, at high speed, 2500 rpm in the experiment, applying varying input voltage method as complement controller in the commutation interval with the reward effectiveness are able to return the unbalanced conditions to the ideal state and improve ripple torque around 42%.

BLDC motor controller applications: The positive characteristics of BLDC motor briefly discussed earlier make them highly attractive for a number of applications in the different areas. Thus, having knowledge about each application and controlling technique used in them has a great importance. Totally, BLDC motor control applications can be classified to three main categories: constant loads, variable loads, and positioning load [80].

Constant load applications: these applications are used more in the cases in which speed change importance is greatly more than fine speed tuning in a special speed. In other words, in these applications no closed-loop control of speed is needed, and open-loop speed controlling on a wide range of speed is possible using motor voltage changing. It should be noticed that the controllers used in these applications only need to know the motor position in six commutations instants, and so inexpensive hall-effect sensors are used.

Increasing or decreasing rate of dynamic motor is not an important issue in these applications, and inexpensive controllers are demanded for these applications.

In addition, in these applications, load directly couples with the motor shaft. It is the distinctive characteristic of these applications group in comparison with two other groups. Some well-known applications of this category can be counted as fans, purifiers [81] and [82], pumps [83], air compressors and blowers [84] and [2].

According to the characteristics counted for these applications, some controllers can be considered as appropriate controllers for these applications like variable dc-link voltage, hysteresis current and PWM without current shaping with two-phase conducting method.

TABLE IV
COMPARATIVE PERFORMANCE VERIFICATION OF TORQUE RIPPLE REDUCTION IN THE DIFFERENT STRATEGIES

Control Method	PWM Frequency	Hysteresis Band	Max	Min	Torque Ripple
Hysteresis Current Control (3-phase mode+shaping)	—	0.1	3.45	3.13	9.70%
Direct Torque Control	—	0.1	3.48	3.10	11.52%
Hysteresis Current Control (2-phase mode+shaping)	—	0.1	3.52	3.13	11.82%
Minimum Copper Losses Control Method	—	0.1	3.51	3.07	13.13%
Hysteresis Current Control (2-phase mode+without shaping)	—	0.1	3.69	3.08	18.48%
PWM Current Control (PWM-ON-PWM)	20000Hz	—	3.61	3.00	18.49%
PWM Current Control (PWM-ON)	20000Hz	—	3.66	2.99	20.30%
PWM Current Control (H-PWM-L-ON)	20000Hz	—	3.68	2.91	23.33%
PWM Current Control (H-ON-L-PWM)	20000Hz	—	3.79	2.71	32.73%
PWM Current Control (ON-PWM)	20000Hz	—	3.84	2.74	33.33%
PWM Current Control (H-PWM-L-PWM)	20000Hz	—	3.97	2.83	34.55%
Current Control Strategy for Creating Virtual DC-Link	20000Hz	—	4.00	2.77	37.27%
Variable DC-Link Voltage Controlling	20000Hz	—	4.20	2.39	54.85%
without using VIVM [*]	—	0.1	4.35	2.64	51.82%
with using VIVM	—	0.1	3.64	3.35	8.79%

*In this case motor speed is 2500 rpm

Variable load applications: in this application category, the load on motor changes in a wide range of speeds and may need delicate speed controlling with proper dynamic response.

In these applications, speed feedback can be semi-closed loop or closed loop performed by advance controlling algorithms that can make the system's spent price increase. Some good examples of these applications can be found in domestic applications like washers, dryers, refrigerators; in aerospace applications like centrifuges, pneumatic devices with electroactuators (EHA/EMA) [85] and [86], pumps, robot arm controlling, gyroscope controlling, marine and population applications [87], marine propulsion [88] systems. Another important application of BLDC motor in this category is the automotive field.

The efficient variable speed feature with low volume of BLDC motors has made them most suited for EVs [89] such as electric cars, buses, pallet trucks, and traction [90]. Likewise, fuel pump controlling [91], electronic wheel controlling, and engine controlling are examples of such applications in the automotive industry.

Hysteresis current controlling methods, PWM with reference current shaping, minimum copper losses controlling, and DTC are some of the best controlling methods in this category.

It should be noted that used controllers in this category of application require accurate position information in each moment because of the requirement for high-performance characteristics; thus, controllers belong to this category use shaft encoder and resolvers to receive speed and position information.

Positional applications: nearly most of the different automation and industrial applications contain some kind of power transmission systems like mechanical gears, gear pump units [92] or timer belts, or a simple belt driven system which belongs to this category. Rapid torque and speed dynamic responses have higher priority in this application category in such a way that frequent reversal of rotation direction may occur successively in a typical cycle that contains acceleration phase, constant speed, and deceleration and positioning.

Since the load on motor can change during each of these phases, used controllers in this part are so complicated that can contain control loops like torque or current, speed and position in addition to speed closed-loop control simultaneously. Optical encoders and synchronous resolvers in these applications are used to measure motor real speed. Identical sensors are used in some of the applications in this category to measure relative positional information. In some other applications, separated positional sensors are used to receive absolute positional information. Some of the most important practical examples of this category are hard disk drives (HDDs) [93] and [94] or DVDs [95] and [96], machine tool servos [97], industrial processors, numerical controlled machines of computer, conveyor controls and hydraulic systems [92].

DTC, hysteresis current controlling with reference current shaping in three-phase conducting mode, and using minimum losses are the proper methods to use for this category of applications.

Electric vehicles and energy regeneration: as it was mentioned in the previous part, one of the most important applications of BLDC motors is in the variable load systems, EV and hybrid electric vehicle (HEV) are two good examples of this application which attracted major industry. It is considered as a variable load because of shifting in vehicle speed dynamic parameters, road slope, weight, and drag coefficient [98]. It should be noticed that used motor drives in EV should not be compared with similar motor drives in industrial processes.

The reason is that EVs drives are compelled to successive start/stop in different conditions, while industrial drives are usually used in their nominal speed.

Most of automobile producer companies like, Toyota, Honda, Ford, and Hyundai, have begun a thorough research for making EVs and HEVs to improve combustion efficiency and environmental consideration. Electrical motors are one of the major energy consumers of EV and HEV; therefore, they should have high efficiency and compact size. Different kinds of electrical motors can be used in the systems of EVs. Because DC motors are in need of periodical repair and service, and because SR motors are of spacious size and of high-level

noise and induction motors require complicated controlling method; thus, car factories have paid their attention to BLDC motors. They don't need usual repair. In addition, they have low noise level, simple controlling method, high efficiency; they also shows faster dynamic response during speed and load changes and have high starting torque [99].

Electric motors used in EVs are classified according to the way of attaching machine wheels to direct-driven and indirect-driven motors. Direct-driven motors, also known as wheel motor or hub motor, directly attach to the wheels and do not need mechanical differential gears.

They have also smaller volume and higher efficiency than indirect-driven motors which are attached to the wheels by mechanical differential gears [100]. Hub-BLDC machines with high efficiency and high performance are designed and used in EV. On the other hand, EV technology declares high efficiency and low environmental pollution, but low-traveled distance is one of the defects. One of the compensation way for this drawback is using energy regeneration controlling system. Electric motor in EV acts as propulsion system.

When motor speed is decreased and negative torque is applied to the electric motor, motor can act as a generator and produce electric power to recharge the battery. In fact, this process as saving and transforming part of kinetic energy to electric energy in energy source is called energy regeneration which is one of the advantages over common one. BLDC motors are good choices for regenerating energy with high efficiency during regenerative braking. Nevertheless, using switching makes the system non-linear as well as battery voltage, the state of the road and vehicle movement cycle is affected by electric brake. All these factors cause change in usual controlling method for regenerative braking [101] and [102]. Among all the motor brake controlling systems, regenerative brake is the only method to save energy in brake control mode which can transform dynamic energy to electrical one during braking and take it back to the source. Therefore, nowadays, regenerative braking is a very important issue, especially in high power range application like EVs and HEVs applications which can return power to the source and should be provided by controlling strategy.

Speed-torque plan has four performance modes in the steady-state. The motor can gain regenerative braking by controlling the movement in the second quarter, at this time the motor will act in power generating state [7].

In the motor state, back-EMF is in phase with the current, and they are 180° degree out of phase in the generator state. Thus, in order to change current direction in the motor winding to produce braking torque, inverter switching sequence should be changed. There are two switching topology for regenerative braking one-switch-active topology and two-switch-active topology [102].

By making the assumption that upper leg switch conducts phase "a" and the lower leg switch conducts phase "c", in the one-switch-active mode only phase "c" lower switch switches, but in the two-switch-active-mode

both mentioned switches continue switching. Energy regeneration is done by the freewheeling diodes of corresponding opposite legs in off-switching mode. It should be mentioned that in the first method no current will be produced by the source in the on-switching mode, but in the second method the source will produce current flows through two on-switches. It causes more energy to regenerate to the battery because of energy saved in the self-inductance in the second method. Stator magnetic field reverses during regenerative braking. Stator and rotor magnetic fields in the motor and generator states are demonstrated in Fig. 32.
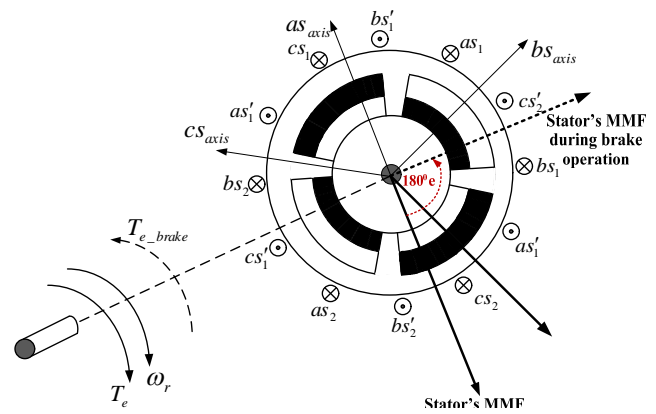

Fig. 32. Stator and rotor magnetic fields in the motor and generator state

Regarding considered controlling method, the magnetic field direction reversing are sensed in the current controlling based methods including PWM and hysteresis by direction change of position sensors and in DTC method which is based on optimum switching in d-q plane, directly sensed and inverter switching sequence changes and the brake and energy regeneration are performed together.

Among verified controlling methods only three methods: DTC, hysteresis current control with reference current shaping in the three-phase conducting mode, and minimum losses are capable of mode changing from motor state to generator state in such a way that they do not need a switching changing mode from motor mode to generator mode, and they can easily adapt their performance automatically to the generator mode.

Therefore, because of the reason mentioned and good torque and speed response characteristic, these methods can be considered as the most proper controlling methods for EVs. Electromagnetic torque responses of the hysteresis current controlling method, DTC, and copper losses minimization for urban moving cycle [103] including accelerating, constant speed, and braking that are depicted in Fig. 33. It should be considered that among these obtaining results, only the speed response of DTC method is shown due to little difference in the speed response settling time of the mentioned methods. As it can be seen in the figures, mentioned methods have very good and fast torque dynamic response, as it is more obvious for DTC method.
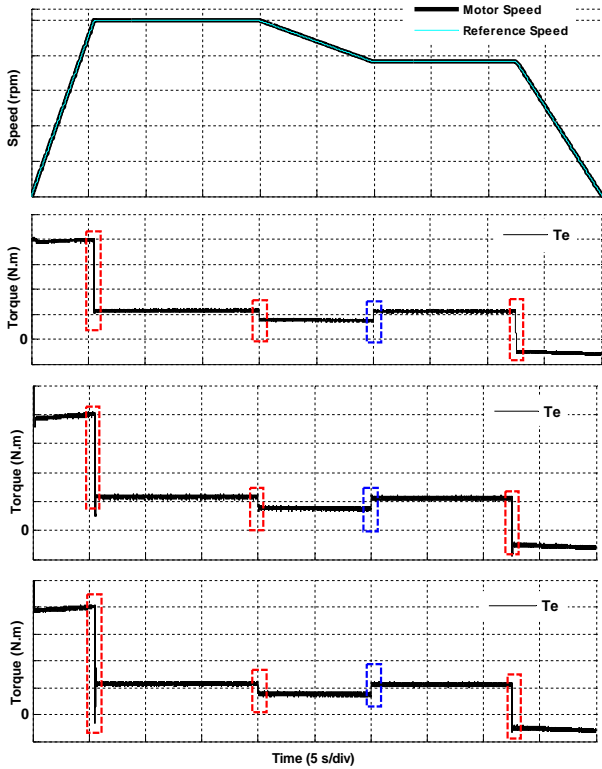
Frequency analysis and BLDC motor drive losses:

Current frequency spectrum and losses are the most important factors in all electrical systems. Unwanted frequency content may cause disturbances in other devices and losses in the motor. From switching frequency point of view, losses in converter and iron losses in the motor are of importance. Losses in the converter are mostly due to the voltage drop on power devices. In a power switch, switching losses depend mainly on dc-link voltage, instantaneous line current and turn-on and turn-off transition times. Semiconductor switches have resistance when they are completely on.

This resistance can result in high drop in power even during very short intervals when the switch is going from non-conductive state to conductive state and vice versa.

These losses cause voltage drop and heating in the system which results in an increase in the system size. It also results in a drop in motor speed and torque.

Drawn currents by BLDC motors are not pure dc currents; moreover, they have notches which produce commutation torque. Regarding that commutation occurs six times in each electrical cycle, the ripple frequency of dc-link current or commutation torque which equals number of notches caused by commutation in per second can be calculated easily as follows:

$$f_{com} = \frac{pN}{20} \qquad (53)$$

Zoomed electromagnetic torque using variable dc-link voltage controlling in the full-load and no-load speeds are shown in Figs. 34 and 35.
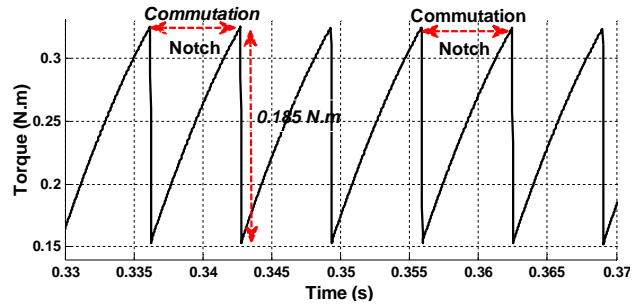

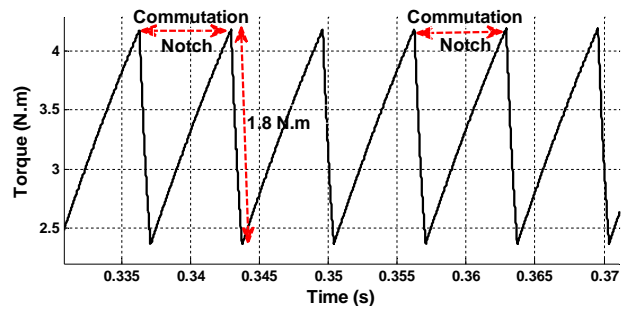Fig. 34. Zoomed electromagnetic torque in no-load speed using variable dc-link voltage control method

Fig. 35. Zoomed electromagnetic torque in full-load using variable dc-link voltage control method

As it can be seen in the figures, torque notches are wide and the relative depth of the notches reaches 57% and 42% of the torque peak in no-load and full-load state respectively. Relative width and depth of the notches decrease along with increase in speed and load, respectively. Dc-link current frequency spectrum, using this method in the no-load and full-load speed is illustrated in Figs. 36 and 37.

It can be deduced from the figures that, if the motor load changes, no change in the fundamental frequency which is around 150 Hz occurs. This frequency is compatible with the calculated one in (53).

It means that, variable dc-link voltage contains no current chopping and in the frequency domain, it only includes harmonics which are produced by current commutation and its frequency is proportional to rotor speed and can be easily calculated by (53). Dc-link voltage frequency spectrum using hysteresis controller in the no-load and full-load state while the speed is kept constant, is depicted in Figs. 38 and 39.

As it is obvious in Fig. 38, the fundamental frequency in the no-load state is around 13.3 kHz, but in the full-load state, maximum fundamental frequency is increased to 18.1 kHz, as equation (36) verifies and Fig. 39 proves it. Therefore, in this control method, commutation notches are no more basic harmonic resources, but, hysteresis controlling switching frequency determines frequency spectrum and switching frequency changes proportional to the changes in applied load to the motor.

It emphasizes major problems of hysteresis controller i.e. difficulty in filtering, unwanted harmonics and inefficiency in the cases in which load torque changes are considerable.
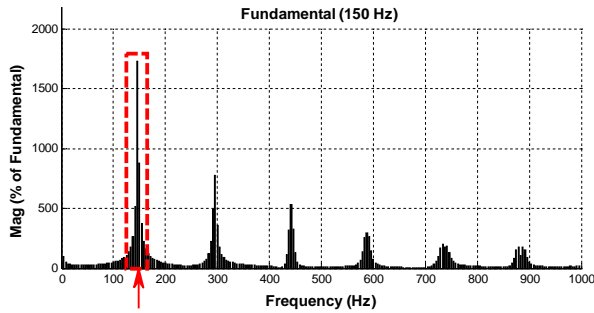

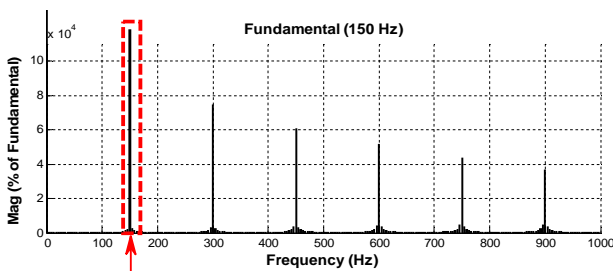Fig. 36. Dc-link current frequency spectrum in no-load speed using variable dc-link voltage control

Fig. 37. Dc-link current frequency spectrum in no-load speed using variable dc-link voltage control
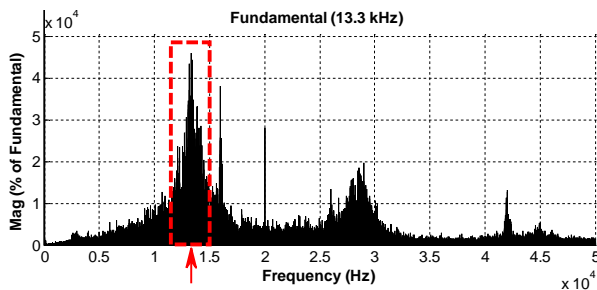

Fig. 38. Dc-link current frequency spectrum in no-load speed using hysteresis control method
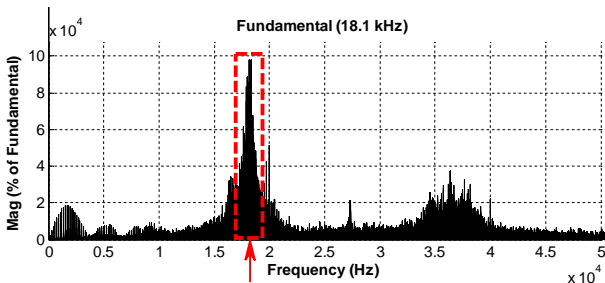

Fig. 39. Dc-link current frequency spectrum in full-load speed using hysteresis control method

Dc-link current frequency spectrum using PWM control method in the identical conditions with the two methods is demonstrated in Figs. 40 and 41. The figures

states that, in this method, frequency content is independent of load. The fundamental frequency is 20 kHz as well as PWM frequency. The other peaks observed in the figure are harmonics of that frequency.
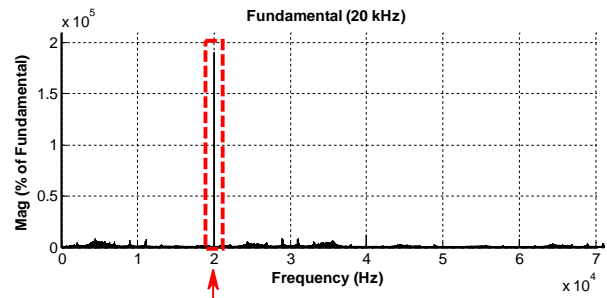

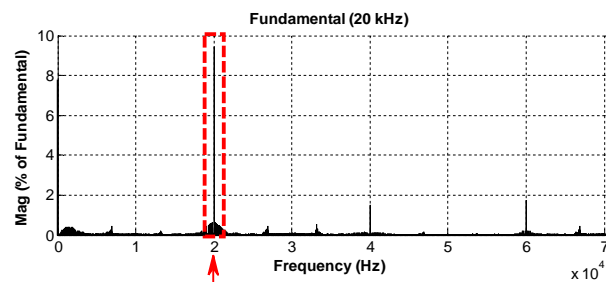Fig. 40. Dc-link current frequency spectrum in no-load speed using PWM control method

Fig. 41. Dc-link current frequency spectrum in full-load speed using PWM control method

The constant frequency of PWM technique during changes in load situations is what has made it more conventional than hysteresis technique and also the filtering of unwanted harmonic is simpler in this technique. Therefore, it can be understood from analysis in frequency domain that dc-link current frequency content is intensively related to the applied load to the motor in the hysteresis control method. This matter is the main reason using this technique in the applications with small load changes. Despite speed error in the steady state in most cases, the PWM control method can be a better choice than hysteresis control method. Variable dc-link voltage control is the only technique that does not produce high-frequency perturbations, at least if voltage source is considered ideal.

From the switching losses point of view, it can be concluded that first, in a few number of cases, if hysteresis band is chosen narrow, uncontrolled switching frequency of hysteresis band technique cannot be acceptable due to high switching losses, but the switching frequency can be tuned by selecting the proper hysteresis band. Totally, in both PWM and hysteresis methods, an increase in switching frequency, on the one hand, causes reduction in torque ripple, and, on the other hand, reduction in switching frequency, unsurprisingly, results in a reduction in switching losses, but in this case the system contains large amounts of low-order harmonics that bulky filter is needed for filtering them. Furthermore, in this situation, they produce high torque

and current ripple which can be unacceptable for the specific application we want to use. Regarding that losses in switching control circuits depend on switch parameters, on the one hand using devices with appropriate characteristics, reduces system total losses, size and expense. On the other hand, choosing optimized switching frequency related to motor and switch characteristics is possible by making a compromise between switching losses and torque ripple. From the frequency analysis point of view and switching frequency, it is possible to gain important advantages compared to the two previously mentioned methods by means of variable dc-link voltage control method. Among the most important advantages for this method, in addition to the point that variable dc-link voltage control method is the best solution in cases we need minimum of switching losses, we can point out to achieving a cheaper single-step power compared to pulsed stage at least when the voltage is not low and the current is not high.

VII. Conclusion

In this paper, a review of basic methods for BLDC motor drive has been presented systematically by means of classified controlling strategies to speed, voltage, current, and torque control accompanied with basic principles of each one. To provide a correct and proper understanding of different drive controlling methods of these types of motors, a simulation study with emphasis on limitations and the characteristics of each method are used. Totally, each method discussed in this paper has its own strengths and weakness from different points of view affecting industry, so none of them is the best choice for BLDC motor drive in all applications. Therefore, in this paper it is tried to discuss different control strategies in appealing viewpoints for the market such as torque ripple, switching losses, and their applications especially EVs.

If a classification of the discussed controlling methods using two-phase conducting mode from the filtering and losses point of view is needed, variable dc-link voltage control method, unipolar PWM, bipolar PWM, and hysteresis current control can be pointed out in an ascending sequence.

Acknowledgements

References

[1] K. W. Lee, D. K. Kim, B. T. Kim, B. I. Kwon, A novel starting method of the surface permanent-magnet BLDC motors without position sensor for reciprocating compressor, *IEEE Trans. Ind. Appl., vol. 44 n. 1*, Jan./Feb. 2008, pp. 85 – 92.

[2] K. Iizuka, H. Uzuhashi, M. Kano, T. Endo, K. Mohri, Microcomputer control for sensorless brushless motor, *IEEE Trans. Ind. Appl., vol. IA-21 n. 4*, May./ June. 1985, pp. 595 – 601.

[3] C. C. Jensen, F. Profumo, T. A. Lipo, A low loss permanent magnet brushless DC motor utilizing tape wound amorphous iron, *IEEE Trans. Ind. Appl., vol. 28 n. 3*, May./ June. 1992, pp. 646 – 651.

[4] R. C. Becerra, M. Ehsani, High-speed torque control of brushless permanent magnet motors, *IEEE Trans. Ind. Electron.* vol. 35 n. 3, August 1988, pp. 402 – 406.

[5] T. Kim, H. W. Lee, M. Ehsani, Position sensorless brushless DC motor/generator drives: review and future trends, *IET Electr. Power Appl., vol. 1 n. 4*, July 2007, pp. 557 – 564.

[6] T. M. Jahns, W.L. Soong, Pulsating torque minimization techniques for permanent magnet AC motor drives-a review, *IEEE Trans. Ind .Electron., vol. 43 n. 2*, April 1996, pp. 321 – 330.

[7] J. W. Dixon, I.A. Leal, Current control strategy for brushless DC motors based on a common DC signal, *IEEE Trans. Power Electron., vol. 17 n. 2*, March 2002, pp. 232 – 240.

[8] H. Tan, S. L. Ho, A novel single current sensor technique suitable for BLDCM drives, *IEEE International Conference on Power Electronics and Drive Systems, ~PEDS 1999~*, July 27-29, 1999.

[9] J. Bocker, Advanced hysteresis control of brushless DC motors, *Deutsch-Koreanisches Symposium*, June, 2004, Aachen.

[10] P. Wipasuramonton, K. Sowsuwan, Current-controlled PWM technique for brushless DC motor drives with a single current sensing resistor, *IEEE 31th International Conference on Telecommunications Energy, ~ INTELEC 2009~*, October 18-22, 2009, Incheon, South Korea.

[11] T. Hui, J. Jian-zhong, W. Xin-yao, W. Yong, A novel current sensor technique for brushless DC motor drives, *Journal of Shanghai University., vol. 4 n. 1*, March 2000, pp. 42– 48.

[12] M. Bonfe, M. Bergo, A brushless motor drive with sensorless control for commercial vehicle hydraulic pumps, *IEEE International Symposium on Industrial Electronics, ~ ISIE 2008~*, June 30 -July 2, 2008, Cambridge, England.

[13] N. Bianchi, S. Bolognani, J. H. Jang, S. K. Sul, Comparison of PM motor structures and sensorless control techniques for zero-speed rotor position detection, *IEEE Trans. Power Electron., vol. 22 n. 6*, March 2007, pp. 2466 – 2475.

[14] T. M. Jahns, Torque production in permanent-magnet synchronous motor drives with rectangular current excitation, *IEEE Trans. Ind. Appl., vol. LA-20 n. 4*, July/August 1984, pp. 803 – 813.

[15] J. Cros, P. Viarouge, Synthesis of high performance PM motors with concentrated windings, *IEEE Trans. Energy Convers., vol. 17 n. 2*, June 2002, pp. 248 – 253.

[16] Z.Q. Zhu, D. Howe, Electrical machines and drives for electric, hybrid, and fuel cell vehicles, *Proceedings of IEEE., vol. 95 n. 4*, April 2008, pp. 746 – 765.

[17] T. Kenjo and S. Nagamori, Permanent-Magnet and Brushless DC Motors (Oxford, U.K. Clarendo, 1985).

[18] T. H. Kim, M. Ehsani, Sensorless control of the BLDC motors from near-zero to high speeds, *IEEE Trans. Power Electron., vol. 19 n. 6*, June 2004, pp. 1635 – 1645.

[19] J. B. Cao, B. G. Cao, Fuzzy-logic-based sliding-mode controller design for position-sensorless electric vehicle, *IEEE Trans. Power Electron., vol. 24 n. 10*, June 2009, pp. 2368 – 2378.

[20] P. Pillay, R. Krishnan, Modeling, simulation, and analysis of permanent-magnet motor drives, Part II: the brushless DC motor drive, *IEEE Trans. Ind. Appl., vol. 25 n. 2*, March/April 1989, pp. 274 – 279.

[21] S. A. KH. Mozaffari Niapour, M. Tabarraie, M. R. Feyzi, Design and analysis of speed-sensorless robust stochastic L∞-induced observer for high-performance brushless DC motor drives with diminished torque ripple, Energy Convers Management, vol. 64, December 2012, pp. 482 – 498.

[22] S. A. KH. Mozaffari Niapour, M. Tabarraie, M. R. Feyzi, A new

robust speed-sensorless control strategy for high-performance brushless DC motor drives with reduced torque ripple, Control Engineering Practice, vol. 24, March 2014, pp. 42 – 54.

[23] T. J. E. Miller, Brushless *Permanent-Magnet and Reluctance Motor Drives* (Oxford, Clarendon Press, 1989).

[24] Duane C. Hanselman, *Brushless Permanent-Magnet Motor Design* (McGraw-Hill, 1994).

[25] D. M. Brod, D.W. Novotny, Current control of VSI-PWM inverters, *IEEE Trans. Ind. Appl., vol. IA-21 n. 4*, May/June 1985, pp. 562 – 570.

[26] T. S. Kim, S.C. Ahn, D .S. Hyun, A new current control algorithm for torque ripple reduction of BLDC motors. *IEEE 27th Annual Conference on Industrial Electronics Society, ~ IECON 2001 ~*, 29 November -02 December, 2001, Denver, USA.

[27] B. Akin, M. Bhardwaj, Trapezoidal control of BLDC motors using hall effect sensors, *Texas Instruments*, 2010.

[28] T.M. Jahns, R.C. Becerra, M. Ehsani, Integrated current regulation for a brushless ECN drive, *IEEE Trans. Power Electron, vol. 6 n. 1*, January 1991, pp. 118 – 126.

[29] S. S. Bharatkar, R. Yanamshetti, D. Chatterjee, A. K. Ganguli, Reduction of commutation torque ripple in a brushless DC motor drive, IEEE 2nd International Conference on Power and Energy, ~ PECon 2008 ~, 1-3 December, 2008, Johor Bahru, Malaysia..

[30] S. J. Park, H. W. Park, M. H. Lee, F. Harashima, A new approach for minimum-torque-ripple maximum-efficiency control of BLDC motor. *IEEE Trans. Ind. Electron, vol. 47 n. 1*, February 2000, pp. 109 – 114.

[31] Z. Xiangjun, C. Boshi, Influences of PWM mode on the current generated by BEMF of switch-off phase in control system of BLDC motor, *IEEE 5th International Conference on Electrical Machines and Systems, ~ ICEMS 2001 ~*, 18-20 August, 2001, Shenyang, China.

[32] W. Kun, R. Junjun, T. Fanghua, Z. Zhongchao, A novel PWM scheme to eliminate the diode freewheeling in the inactive phase in BLDC motor, *IEEE 35th Annual Conference on Power Electronics Specialists, ~ PESC 04 2004 ~*, 20-25 June, 2004.

[33] Z. Xiangjun, C. Boshi, Z. Pingping, L. Huaigang, A new method to minimize the commutation torque ripple in trapezoidal BLDC motor with sensorless drive, *IEEE 3rd International Conference on Power Electronics and Motion Control, ~ IPEMC 2000 ~*, 15-18 August, 2000, Beijing, China.

[34] Q. Li, H. Huang, B. Yin, The study of PWM methods in permanent magnet brushless DC motor speed control system, *IEEE International Conference on Electrical Machines and Systems, ~ ICEMS 2008 ~*, 17-20 October, 2008, Wuhan, China.

[35] Y. S. Lai, F. S. Shyu, Y. K. Lin, Novel PWM technique without causing reversal dc-link current for Brushless DC motor drives with bootstrap driver, *IEEE 40th International Conference on Industry Applications ~ IAS 2005 ~*, 2-6 October, 2005.

[36] J.Y. Hung, Z. Ding, Design of currents to reduce torque ripple in brushless permanent magnet motors, *IEE Electric Power Applications., vol. 140 n. 4*, July 1993, pp. 260 – 266.

[37] D.C. Hanselman, Minimum torque ripple, maximum efficiency excitation of brushless permanent magnet motors, *IEEE Trans. Ind. Electron., vol. 41 n. 3*, June 1994, pp. 292 – 300.

[38] F. Piriou, A. Razek, R. Perret, and H. Le-Huy, Torque characteristics of brushless DC motors with imposed current waveform, *IEEE Annual Meeting on Industry Applications ~ IAS 1986 ~*, September, 1986.

[39] C. Marchland, A. Razek, Optimal torque operation of digitally controlled permanent magnet synchronous motor drives, *IEE Electric Power Applications., vol. 140 n. 3*, May 1993, pp. 232 – 240.

[40] S. Clenet, Y. Lefevre, N. Sadowski, S. Astier, M. L. Mazenc, Compensation of permanent magnet motors torque ripple by means of current supply wave shapes control determined by finite element method. *IEEE Trans. Magn.., vol. 29 n. 2*, March 1993, pp. 2019 – 2023.

[41] Z.Q. Zhu, Y. Liu, D. Howe, Comparison of performance of brushless DC drives under direct torque control and PWM current control, *IEEE 80th International Conference on Electrical Machines and Systems ~ ICEMS 2005 ~*, 29 September, 2005, Wuhan, China.

[42] T. Kenjo, S. Nagamori, *Permanent Magnet and Brushless DC Motors* (Clarendon Press, 1984).

[43] J. R. Hendershot, Miller, *Design of Brushless Permanent-Magnet Motors* (Oxford Univ. Press, 1994).

[44] G. Jang, M. G. Kim, A bipolar-starting and unipolar-running method to drive a hard disk drive spindle motor at high speed with large starting torque, *IEEE Trans. Magn.., vol. 41 n. 2*, February h 2005, pp. 292 – 300.

[45] G. Yan, N. Fusun, O. Serteller, Brushless direct current (BLDC) machine bipolar–unipolardriving circuit education study, *Procedia Social and Behavioral Sciences, vol. 2 n. 2*, January 2010, pp. 2694 – 2699.

[46] J. Faiz, M. R. Azizian, M. Aboulghasemian-Azami, Simulation and analysis of brushless DC motor drives using hysteresis, ramp comparison and predictive current control techniques, *Simulation Practice and Theory, vol. 3 n. 6*, January 1996, pp. 347 – 363.

[47] L. Malesani, L. Rossetto, P. Tomasin, A. Zuccato, Digital adaptive hysteresis current control with clocked commutations and wide operating range, *IEEE Trans. Ind. Appl., vol. 32 n. 2*, March/April 1996, pp. 316 – 325.

[48] D. M. E. Ingram, S. D. Round, A fully digital hysteresis current controller for an active power filter, *International Journal of Electronics., vol. 86 n. 10*, October 1999, pp. 1217 – 1232

[49] A. Moussi, A. Torki, An Improved efficiency permanent magnet brushless DC motor pv pumping system, *Larhyss Journal., vol. 1 n. 1*, May 2002, pp. 139 – 156.

[50] P. C. Desai, A. Emadi, A novel digital control technique for brushless DC motor drives: current control, *IEEE International Conference on Electric Machines and Drives,* 19 May, 2005, San Antonio, USA.

[51] M.F. Rahman, K.S. Low, K.W. Lim, Approaches to the control of torque and current in a brushless DC drive, *IEEE 6th International Conference on Electric Machines and Drives,* 8-10 September, 1993, Oxford, England.

[52] Texas Instruments Europe, DSP Solutions for BLDC Motors, March 1997.

[53] T. Kim, H. W. Lee, L. Parsa, M. Ehsani, Optimal power and torque control of a brushless DC (BLDC) motor/generator drive in electric and hybrid electric vehicles, *IEEE 41st Annual Meeting on Industry Applications, ~ IAS 2006 ~,* 8-12 October, 2006, Tampa, USA.

[54] N. Gaurav, C. K. Narayanr, A survey and comparison of characteristics of motor drives used in electric vehicles, *IEEE Canadian Conference on Electrical and Computer Engineering, ~ CCECE 2006 ~,* May, 2006, Ottawa, Canada.

[55] K.T. Chau, C. C. Chan, Chunhua Liu, Overview of permanent-magnet brushless drives for electric and hybrid electric vehicles, *IEEE Trans. Ind. Electron, vol. 55 n. 6*, June 2008, pp. 2246 – 2257.

[56] G. MadhusudhanaRao, B.V.SankerRam, Kumar B.Smapath, Kumar K.Vijay, Speed Control of BLDC Motor Using DSP, *International Journal of Engineering Science and Technology, vol. 2 n. 3*, November 2010, pp. 143 – 147.

[57] G. MadhusudhanaRao, B.V.SankerRam, Speed control of BLDC motor with common current. *International Journal of Engineering Science and Technology, vol. 2 n. 6*, November 2009, pp. 182 – 187.

[58] Kyeong-Hwa Kim, Myung-Joong Youn, Performance comparison of PWM inverter and variable DC link inverter schemes for high-speed sensorless control of BLDC motor, *Electronics Letters., vol. 38 n. 21*, October 2002, pp. 1294 – 1295.

[59] J. Musil, 3-Phase BLDC Drive Using Variable DC Link Six-Step Inverter. May 2006, Available: http://www. freescale.com.

[60] I. Takahashi, T. Koganezawa, G. Su, K. Oyama, A super high speed PM motor drive system by a quasi-current source inverter, *IEEE Annual Meeting on Industry Applications, ~ IAS 1993 ~,* 2-8 October, 1993, Toronto, Canada.

[61] Rashid, M. H., *Power Electronics - Circuits, Devices, and Applications* (Prentice-Hall, Ltd., 1988).

[62] D. K. Kim, K. W. Lee, B.I. Kwon, Commutation torque ripple reduction in a position sensorless brushless DC motor drive, *IEEE Trans. Power Electron., vol. 21 n. 6*, November 2006, pp. 1762 – 1768.

[63] R. Carlson, M. Lajoie-Mazenc, J. C. dos S. Fagundes, Analysis of torque ripple due to phase commutation in brushless dc machines, IEEE Trans. Ind. Appl., vol. 28 n. 3, May/June 1992, pp. 632 – 638.

[64] H. Lu, L. Zhang, W. Qu, A new torque control method for torque ripple minimization of BLDC motors with un-ideal back EMF, *IEEE Trans. Power Electron., vol. 23 n. 2*, March 2008, pp. 950 – 958.

[65] Guangwei Meng, Hao Xiong, Huaishu Li, Commutation torque ripple reduction in BLDC motor using PWM-ON-PWM mode, *IEEE International Conference on Electrical Machines and Systems ~ ICEMS 2009 ~*, 15-18 November, 2009, Tokyo, Japan.

[66] K. Y. Nam, W.T. Lee, C. M. Lee, J.P. Hong, Reducing torque ripple of brushless DC motor by varying input voltage, *IEEE Trans. Magn., vol. 42 n. 4*, April 2008, pp. 1307 – 1310.

[67] Y.A. Chapuis, D. Roye, J. Davoine, Principles and implementation of direct torque control by stator flux orientation of an induction motor, *IEEE 10th Conference on Applied Power Electronics ~ APEC 1995 ~*, 5-9 March, 2009, Dallas USA.

[68] J. N. Nash, Direct torque control, induction motor vector control without an encoder, *IEEE Trans. Ind. Appl., vol. 33 n. 2*, March/April 1997, pp. 333 – 341.

[69] Y. Liu, Z. Q. Zhu, D. Howe, Direct torque control of brushless DC drives with reduced torque ripple. *IEEE Trans. Ind. Appl., vol. 41 n. 2*, March/April 2005, pp. 599 – 608.

[70] S. B. Ozturk, W. C. Alexander, H. A. Toliyat, Direct torque control of four-switch brushless DC motor with non-sinusoidal back EMF, *IEEE Trans. Power Electron., vol. 25 n. 2*, February 2010, pp. 263 – 271.

[71] S. B. Ozturk, H. A. Toliyat, Direct torque control of brushless dc motor with non-sinusoidal back-EMF, *IEEE International Conference on Electric Machines & Drives ~ IEMDC 2007 ~*, 3-5 May, 2007, Antalya, Turkey.

[72] Mirzaei, H., Pahlavani, M.A., Naderi, P., Comparison of direct torque control of BLDC motor with minimum torque ripple in four and six-switch inverters, (2013) *International Review of Electrical Engineering (IREE),* 8 (3), pp. 971-980.

[73] Y. Liu, Z. Q. Zhu, D. Howe, Instantaneous torque estimation in sensorless direct torque controlled brushless DC motors, *IEEE Trans. Ind. Appl., vol. 43 n. 5*, October 2005, pp. 1275 – 1283.

[74] C. C. Chan, J. Z. Jiang, W. Xia, K. T. Chau, Novel wide range speed control of permanent magnet brushless motor drives, *IEEE Trans. Power Electron., vol. 10 n. 5*, September 1995, pp. 539 – 546.

[75] Y. H. Lim, Y. S. Kook, Y. Ko, A new technique of reducing torque ripples for BDCM drives, *IEEE Trans. Ind. Electron., vol. 44 n. 5*, October 1997, pp. 735 – 739.

[76] Z. Q. Zhu, S. Ruangsinchaiwanich, N. Schofield, D. Howe, reduction of cogging torque in interior-magnet brushless machines, *IEEE Trans. Magn., vol. 39 n. 5*, September 2010, pp. 3238 – 3240.

[77] T. Sebastian, V. Gangla, Analysis of induced EMF waveforms and torque ripple in a brushless permanent magnet machine, *IEEE Trans. Ind. Appl., vol. 32 n. 1*, January/February 1996, pp. 195 – 200.

[78] N. Bianchi, S. Bolognani, Design techniques for reducing the cogging torque in surface-mounted PM motors, *IEEE Trans. Ind. Appl., vol. 38 n. 5*, September 2002, pp. 1259 – 1265.

[79] M. S. Islam, S. Mir, T. Sebastian, Issues in reducing the cogging torque of mass-produced permanent-magnet brushless DC motor, *IEEE Trans. Ind. Appl., vol. 40 n. 3*, May/June 2004, pp. 813 – 820.

[80] P. Yedamale, *Brushless DC (BLDC) Motor Fundamentals* (Microchip Technology, Inc., 2003).

[81] R. Krishnan, S. Lee, PM brushless DC motor drive with a new power-converter topology, *IEEE Trans. Ind. Appl., vol. 33 n. 4*, July/August 1997, pp. 973 – 982.

[82] C. H. Chen, M. Y. Cheng, A new cost effective sensorless commutation method for brushless DC motors without phase shift circuit and neutral voltage, *IEEE Trans. Power Electron., vol. 22 n. 2*, March 2007, pp. 644 – 653.

[83] S. A. KH. Mozaffari Niapour, S. Danyali, M. B. B. Sharifian, M. R. Feyzi, Brushless DC motor drives supplied by PV power system based on Z-source inverter and FL-IC MPPT, *Energy Convers Management, vol. 52 n. 8-9*, August 2011, pp. 3043 – 3059.

[84] H. G. Yee, C. S. Hong, J. Y. Yoo, H. G. Jang, Y. D. Bae, Y. S. Park, Sensorless drive for interior permanent magnet brushless DC motors, *IEEE International Conference on Electric Machines & Drives ~ IEMDC 1997 ~*, 18-21 May, 1997, Milwaukee, USA.

[85] T. M. Jahns, R. C. Van Nocker, High-performance EHA controls magnet interior permanent magnet motor. *IEEE Trans. Aerospace and Electronic Systems, vol. 26 n. 3*, May 1990, pp. 534 – 542.

[86] V. Hubik, M. Sveda, V. Singule, On the development of BLDC motor control run-up algorithms for aerospace application, *IEEE 13th International Conference on Power Electronics and Motion Control ~ EPE-PEMC 2008 ~*, 1-3 September, 2008, Poznan, Poland.

[87] Kolahdooz, A., Shakeri, M., A new BLDC motor for propulsion application, (2010) *International Review of Electrical Engineering (IREE),* 5 (5), pp. 1872-1878.

[88] B. Singh, Recent advances in permanent magnet brushless DC motors, *Sadhana., vol. 22 n. 6*, December 1990, pp. 837 – 853.

[89] M. Naidu, T.W. Nehl, S. Gopalakrishnan, L. Wurth, Keeping cool while saving space and money: a semi-integrated, sensorless PM brushless drive for a 42-V automotive HVAC compressor, *IEEE Industry Applications Magazine, vol. 11*, July/August 2005, pp. 20 – 28.

[90] B. Sneyers, G. Maggetto, J. Van Eck, Inverter fed permanent magnet motor for road electric traction, *IEEE International Conference on Electrical Machines and Systems, ~ ICEMS 1992 ~*, , 1992.

[91] J. Shao, D. Nolan, M. Teissier, D. Swanson, A novel microcontroller-based sensorless brushless DC (BLDC) motor drive for automotive fuel pumps, *IEEE Trans. Ind. Appl., vol. 39 n. 6*, November/December 2003, pp. 1734 – 1740.

[92] M. Bonfe, M. Bergo, A brushless motor drive with sensorless control for commercial vehicle hydraulic pumps, *IEEE International Symposium on Industrial Electronics ~ ISIE 2008 ~*, 30 June -2 July, 2008, Cambridge, England.

[93] Q. Jiang, Chao Bi, R. Huang, A new phase-delay-free method to detect back EMF zero-crossing points for sensorless control of spindle motors*, IEEE Trans. Magn., vol. 41 n. 7*, July 2005, pp. 2287 – 2294.

[94] W. J. Lee, S. K. Sul, A new starting method of BLDC motors without position sensor, *IEEE Trans. Ind. Appl., vol. 42 n. 6*, November/December 2006, pp. 1532 – 1538.

[95] Y. S. Lai, F. S. Shyu, Y. H. Chang, Novel pulse-width modulation technique with loss reduction for small power brushless DC motor drives, *IEEE 37th Annual Meeting on Industry Applications ~ IAS.2002 ~*, 13-18 October, 2002, Pittsburgh, USA.

[96] Y. S. Lai, F. S. Shyu, Y. H. Chang, Novel loss reduction pulse width modulation technique for brushless dc motor drives fed by MOSFET inverter, *IEEE Trans. Power Electron., vol. 19 n. 6*, November 2005, pp. 1646 – 1652.

[97] I. Takahashi, T. Koganezawa, G. Su, K. Oyama, A super high speed PM motor drive system by a quasi-current source inverter, *IEEE Annual Meeting on Industry Applications Society ~ IAS.1993 ~*, 2-8 October, 1993, Toronto, Canada.

[98] K. L. Butler, M. Ehsani, P. Kamath, A matlab-based modelling and simulation package for electric and hybrid electric vehicle design. *IEEE Trans. Vehicular Technology, vol. 48 n. 6*, November 1999, pp. 1770 – 1778.

[99] G. Nanda, N. C. Kar, A survey and comparison of characteristics of motor drives used in electric vehicles, *IEEE Canadian Conference on Electrical and Computer Engineering ~ CCECE 2006 ~*, May, 2006, Ottawa, Canada.

[100] N. A. Rahim, W. P. Hew, M. Tadjuddin, Design of axial flux permanent magnet brushless DC motor for direct drive of electric vehicle, *IEEE Canadian Conference on Electrical and Computer Engineering ~ CCECE 2006 ~*, May, 2006, Ottawa, Canada.

[101] S. Onoda, A. Emadi, PSIM-based modelling of automotive power systems: conventional, electric, and hybrid electric vehicles, *IEEE Trans. Vehicular Technology, vol. 53 n. 2*, March 2004, pp. 390 – 400.

[102] R. C. Becerra, M. Ehsani, T. M. Jahns, Four-quadrant brushless

ECM drive with integrated current regulation, *IEEE Trans. Ind. Appl., vol. 28 n. 4*, July/August 1992, pp. 833 – 841.

[103] J. Larminie, J. Lowry, *Electric Vehicle Technology Explained* (John Wiley and Sons, Ltd., 2003).

Authors' information

[1]Department of Electrical and Computer Engineering, University of Illinois at Chicago, Chicago, IL. 60607, USA.

[2]Private Research Laboratory, 71557, Shiraz, Iran.

[3]Research Department of Fars Power Maintenance Company, Shiraz, Iran.

[4]Faculty of Electrical and Computer Engineering, University of Tabriz, 51664, Tabriz, Iran.

[5]Faculty of Engineering, Ilam University, Ilam, Iran.

[6]Department of Electrical and Computer Engineering, University of North Carolina at Charlotte, Charlotte, NC. 28223, USA.

Seyedabdolkhalegh Mozaffari Niapour was born in Shiraz, Iran, on July 23, 1984. He received the B.Sc. degree (first-class Hons.) from the Islamic Azad University, Kazerun, Iran, in 2007, and the M.Sc. degree (first-class Hons.) from the University of Tabriz, Tabriz, Iran, in 2011, both in electrical power engineering. He is currently working towards his PhD degree at the Department of Electrical and Computer Engineering, University of Illinois at Chicago, Chicago, IL, USA. His main research interests include permanent-magnet brushless dc motor drives, adjustable speed drives, power electronic converters, electric and hybrid vehicles, and renewable energy systems. He currently focuses on sensorless control of high-performance brushless dc motor drives and single stage multi input converters. Mr. Mozaffari Niapour is a member of Organization of Exceptional Talents at University of Tabriz and a professional member of the Institute of Electrical and Electronics Engineers (IEEE).

Ghasem Shokri Garjan was born in Ardabil, Iran, on April 24, 1984. He received the B.Sc. degree in electrical engineering from Azad University, Ardabil, Iran in 2008, and the M.Sc. degree in electrical engineering from University of Tabriz, Tabriz, Iran in 2011. His research interests include electric and hybrid vehicles, permanent-magnet brushless dc motors, adjustable speed drives, and power electronics. Mr. Shokri Garjan is a student member of the Institute of Electrical and Electronics Engineers (IEEE).

Mehdi Shafiei was born in Shiraz, Iran in 1987. He received the B.Sc degree in Control engineering from the Shiraz University of Technology, Shiraz, Iran in 2009 and M.S degree in electrical machine and drives, Tabriz, Iran in 2011 with first honor degree. Aftar his graduation he joined Fars Science and Research Branch, Islamic Azad University as a lectrurer. Also he joined Niroo Research Institute and Fars Power Maintenance Company as a researcher. His research interests include drive and design of permanent-magnet brushless DC machines, electric and hybrid vehicles, renewable energy systems, intellgent algorithms, and adaptive and robust controller. Mr. Shafiei is a member of Organization of Exceptional Talents at University of Tabriz and a professional member of the Institute of Electrical and Electronics Engineers (IEEE).

Mohammad Reza Feyzi received his BSc and MSc in 1975 from university of Tabriz in Iran with honor degree. He worked in the same university during 1975 to 1993. He started his PhD work in the University of Adelaide, Australia in 1993. Soon after his graduation, he rejoined to the University of Tabriz. He worked as an assistant professor at Ryerson University during 2003-2004. Currently, he is a professor in the University of Tabriz in Iran. His research interests are finite element analysis, design and simulation of electrical machines and transformers.

Saeed Danyali was born in Abdanan, Ilam, Iran in 1983. He received the B.Sc. degree in electronic engineering from the University of Yazd, Yazd, Iran, in 2005, the M.Sc. and Ph.D. degrees in electrical power engineering from the University of Tabriz, Tabriz, Iran, in 2008 and 2013, respectively. In 2013, he joined the Faculty of Engineering, Ilam University, Ilam, Iran, where he has been an Assistant Professor since 2013. His research interests are the areas of renewable energy systems, power electronic converters, brushless dc motor drives, and electric and hybrid vehicles. Dr. Danyali currently focuses on the single stage multi input converters.

Mojtaba Bahrami Kouhshahi was born in Sirjan, Iran in 1984. He received his B.Sc. degree in Power engineering from the Shahid Bahonar University of Kerman, Kerman, Iran in 2008, and his M.Sc. in Electrical Machine and Drives from Tabriz University, Tabriz, Iran in 2011. He is currently working towards his PhD degree at the Department of Electrical and Computer Engineering, University of North Carolina at Charlotte, Charlotte, NC, USA. His research interests include finite element analysis and design of electric machines, brushless dc motor drives and generators, adjustable speed drives and renewable energies. Mr. Bahrami is a member of Organization of Exceptional Talents at University of Tabriz and a professional member of the Institute of Electrical and Electronics Engineers (IEEE).